Organically-modified silica aerogels: a density functional theory study

Pedro Maximiano[a,**], Luísa Durães[a], Pedro Simões[a,*]

[a] *CIEPQPF, Department of Chemical Engineering, University of Coimbra, Rua Sílvio de Lima, 3030-790 Coimbra, Portugal*

Abstract

The primary particles of silica aerogels resulting from three different mixtures of precursors – 50% tetramethylorthosilicate (TMOS)/50% vinyltrimethoxysilane (VMTS); 50% tetraethylorthosilicate (TEOS)/50% aminopropyltriethoxysilane and 50% TEOS/50% glycidylpropoxi – as well as aerogels of pure TMOS and VTMS, have been studied by quantum mechanics density functional theory calculations (DFT), at the B3LYP/6-311+G(d,p) level of theory). Thermo-chemical calculations have indicated that cage structures are the most favored for all materials, followed by other species (linear and cyclic) with high degrees of condensation. A vibration mode analysis based on a numerical model fitted to experimental infrared spectra, has allowed the identification of the most representative silica clusters for all the materials studied. The resulting theoretical spectra were close to their experimental counterparts. Analysis of calculated and experimental ^{29}Si-NMR spectral data generally corroborated the derived model.

Keywords: Silica aerogels, Molecular modeling and simulation, Density functional theory, ORMOSIL aerogels.

Abbreviations. APTES - aminopropyltriethoxysilane; B3LYP - Becke, three-parameter, Lee-Yang-Parr (functional); DFT - density functional theory; GIAO - Gauge Including Atomic Orbital; GLYMO - 3-glycidyloxypropiltrimethoxysilane; MTMS - methyltrimethoxysilane; ORMOSIL - organically-modified silica aerogels; TEOS - tetraethylorthosilicate; TMOS - tetramethylorthosilicate; TMS - tetramethylsilane VTMS - vinyltrimethoxysilane;

*Corresponding author. Tel.: +351-239798732, E-mail adress: pnsim@eq.uc.pt
**Corresponding author. Tel.: +351-239798702, E-mail adress: pmsantos@eq.uc.pt

1. Introduction

Ever since their discovery by Kistler in 1931[1], silica aerogels have been the focus of intense academic research and have also gathered great interest from industrial circles for a variety of applications.[2] Due to their extremely low thermal conductivity (as low as 0.010 $W.m^{-1}.K^{-1}$) combined with a very low density (<0.1 $g.cm^{-3}$), these materials have now come of age in the aerospace industry, being used primarily as thermal insulators for spacecraft.[2–4] Their high porosity (80 - 99.8%) and surface area (500 - 1200 $m^2.g^{-1}$) result in exceptional performance as adsorbents for organic pollutants and heavy metals, catalytic supports, drug delivery, among others.[5] Furthermore, the good optical properties and in particular the low refractive index presented by silica aerogels (1.007 - 1.25) have, for instance, opened the route for their use in Cherenkov detectors.[2, 6]

Silica aerogels can be easily synthesized in mild conditions by the sol-gel process. Silicon-bearing precursor molecules, typically in the form of alkoxides, such as tetramethylorthosilicate (TMOS), are first hydrolyzed, as alkoxide groups are converted to reactive hydroxyl groups. Then, condensation reactions between these groups take place, leading to the formation of primary particles which cluster into secondary particles, resulting in a sol.[2] Upon further condensation, the particles link to each other, forming a 3D porous gel network, with a "pearl necklace" structure possessing meso and micropores. An aging step is then typically performed, from which the links between particles are reinforced. This is followed by one of three drying methods: (a) supercritical drying, either by removing the solvent in supercritical conditions or by extraction with supercritical CO_2; (b) freeze-drying, by solvent sublimation, resulting in cryogels; (c) evaporative drying, vaporizing the solvent. Although silica aerogels have traditionally been prepared by supercritical drying procedures, evaporative drying techniques where capillary stresses are reduced can also lead to aerogels with minimal shrinkage.[7]

In spite of the many exceptional properties of silica aerogels, these materials possess severe issues that render production at commercial scales extremely difficult, in particular with regards to their very poor mechanical resistance. This is related to the fragile micro-structure of the aerogel matrix, given that the secondary particles are linked by narrow bridges (necks) that can easily break.[4] Also related to this problem is the fact that silica aerogels tend to shed particles[8], which is undesirable in the strictly clean environments upon which aerospace components are typically assembled.

So far, intensive research has been devoted to the mechanical reinforcement of silica aerogels, by strengthening the connections between silica particles. The versatility of sol-gel chemistry allows for the incorporation of silica precursors of different chemical composition, such as those represented in Figure 1, resulting in organically-modified silica (ORMOSIL) aerogels. For instance, the use of methyltrimethoxysilane (MTMS) allowed improved mechanical resistance and hydrophobicity, while vinyltrimethoxysilane (VTMS) also enhances hydrophobicity, prevents particle shedding, and allows the tailoring of the pore size of these materials by changing reaction conditions.[9–13] Mechanical reinforcement can also be accomplished by incorporating other materials in the aerogel matrix, such as polymers and fibers.[4] It is often the case that organic modifications of the silica matrix are required for compatibilization of both phases of the composite materials. For example, the use of VTMS in the matrix provides vinyl moieties that are grafting points for subsequent polymerization processes, while aminopropyltriethoxysilane (APTES) and 3-glycidyloxypropiltrimethoxysilane (GLYMO) also possess moieties that can react with other functional groups, thus enabling the establishment of organic links

between silica particles.[12, 14, 15]

The successful development of materials based on silica gels requires fundamental knowledge about the processes that govern their formation at a microscopic level. In the last few decades molecular modeling and simulation methods have become an invaluable tool for product design in materials science, as they are able to provide insights into complex chemical and physical phenomena.[16, 17] So far, these tools have been extensively employed for the study of unmodified silica aerogels, i.e. those derived from TMOS/TEOS. For instance, quantum mechanics calculations have clarified the mechanisms of hydrolysis and condensation reactions of silica precursors both in acidic and basic conditions[18–21], as well as giving a description of the distribution of silica clusters (primary particles) formed in the first stages of the sol-gel process[22, 23]. At the nanoscale domain, all-atom and coarse-grained molecular dynamics simulations have elucidated the process of silica nucleation and the formation of the 3D network.[24–28]

However, this picture is not so clear in the case of ORMOSIL aerogels. The introduction of organic groups of different nature in the system in the place of hydroxyl groups can result in significant changes in the chemistry of the early stages of the sol-gel process and in the also relevant physical interactions of the latter stages. So far there have been very few molecular modeling and simulation studies of ORMOSIL aerogels[29–31], and experimental data alone does not give enough detail to fully answer these questions. In this work, spectroscopic data (FTIR and solid-state ^{29}Si NMR) of ORMOSIL aerogels of three chemical compositions – 50% TMOS/50% VTMS (hence abreviatted as TMVT), 50% TEOS/50% APTES (abbreviated as TMAP) and 50% TEOS/50% GLYMO (hence given the name TMG) – with actual interest[32] have been theoretically studied based on density functional

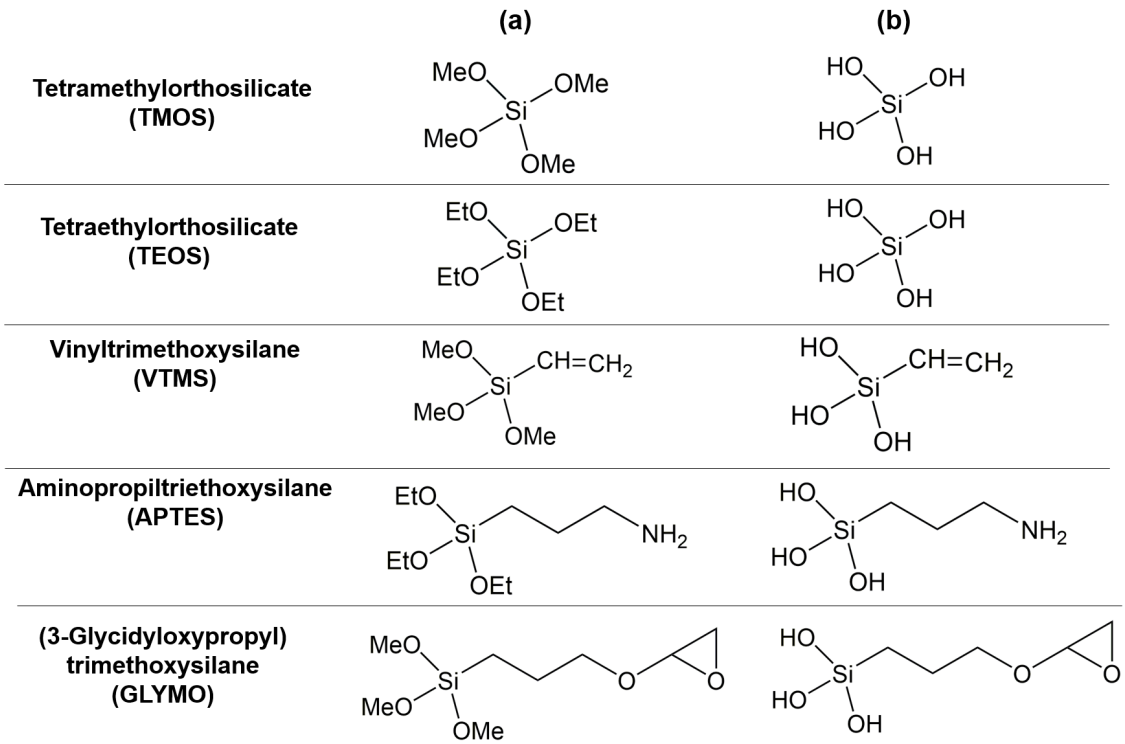

Figure 1: Examples of silica precursors for the synthesis of ORMOSIL aerogels: (a) structure of the precursor and (b) structure after full hydrolysis of alkoxide groups. The materials derived from mixtures of these precursors were the object of study of this work.

theory (DFT) calculations in order to gain insights into the type of structures present at the initial steps of the synthesis of these materials. Apart from its own relevance within the sub-nanometric domain (from molecular to supramolecular scale), this work also lays ground for subsequent molecular dynamics studies at nanoscale and beyond.

2. Methods

Silica aerogels generated from the three different compositions were studied by considering a large set of possible clusters (oligomers) that can be derived from condensation reactions occurring between their respective silica precursors, assuming that they have been completely hydrolyzed prior to such reactions. This set of possible silica clusters, listed in Tables A.1, A.2 and A.3 (Supporting Information, S.I.), was built in accordance with a previous work done by our research group[30], considering the following types of structures: (a) linear structures, with or without ramifications, with 2 to 8 Si atoms; (b) cyclic structures, with or without ramifications, with 2 to 4 Si atoms; (c) cage-like structures, consisting of 8 Si atoms disposed in a cubic-shaped configuration. The structures are labeled according to the Q^n_m notation, where n represents the number of Si atoms that are bonded by bridging m oxygen atoms[29, 30]. For each structure considered in these groups, up to six geometric isomers were considered (corresponding to different positions of the hydroxyl groups and the organic substituent groups - vinyl in the case of VTMS, aminopropyl for APTES, and glycidylpropoxy in GLYMO). Whenever possible, higher molecular symmetry groups were also studied (otherwise the default group was C1).

Each cluster in the set was then theoretically studied by starting with a rough conformational search with the MMFF94 forcefield followed by a geometry optimization with the semi-empirical method PM3. The subsequent computations (geometry optimizations and theoretical spectra) were performed using the package Gaussian 09[33], in vacuum, mostly at the B3LYP/6-311+G(d,p) level of theory. The absence of imaginary frequencies was used to confirm that each optimized structures was in fact a minimum in the potential energy surface. The thermochemical data derived from vibrational analysis allowed to determine the most stable configuration (conformer) of a given cluster.

The ^{29}Si-NMR chemical shifts were calculated for the most stable configurations, using the Gauge Including Atomic Orbital (GIAO)[34, 35] and the B3LYP functional with the IGLO-III triple zeta basis set[36, 37]. The theoretical chemical shifts were then computed relative to the shielding of tetramethylsilane (TMS, $\delta_{\mathrm{Si}} = 330.18$ ppm) calculated at the same B3LYP/IGLO-III level of theory.

Experimental details on spectroscopic data and related methods (FTIR and solid-state ^{29}Si NMR) invoked along with the discussion can be found in S.I.

3. Results and discussion

3.1. Energetic analysis

The first part of this study was targeted to find the most stable silica primary particles (clusters) that can be present in the three aerogel compositions considered as a result of the first stages of the condensation process. To this end, a vast set of possible clusters was identified and their geometries and energies computed at the B3LYP/6-311+G(d,p) levels of theory. The electronic energies, Gibbs

free energies, rotational constants and dipole moments for the all the clusters of TMVT, TMAP and TMG (as listed in Tables S1, S2 and S3) are gathered in A.4, A.5 and A.6 (S.I.), respectively. These energies were then compared, and the minimum energy configuration for each type of cluster has been highlighted in bold, with the difference in total energy (ΔE_{total}) and Gibbs free energy (ΔG) relative to this configuration being computed. Most of the species with the minimum total energy also exhibit a minimum Gibbs free energy, but this is not always the case. As such, the silica cluster considered to be the most stable was that which presents the minimum Gibbs free energy. The optimized geometries for the most stable conformers of each cluster can be found in figures A.1, A.2 and A.3 (S.I.) for the TMVT, TMAP and TMG aerogels, respectively. For all these compositions, it was observed that linear species with a high degree of condensation ($Q_3^1Q_1^3Q_1^2$, $Q_2^3Q_4^1$, $Q_1^4Q_1^3Q_5^1$, $Q_2^3Q_2^2Q_4^1$) possess a high number of intramolecular hydrogen bonds in virtue of a high concentration of exposed hydroxyl groups. In some of the clusters of TMAP and TMG it was noted that terminal amine groups and epoxy or ether groups, respectively, also participate in intramolecular hydrogen bonds, which are made possible by the flexibility of the alkane chain which links them to the Si atom. It is also worth noting that some configurations of higher symmetry led to saddle points which, once the imaginary frequency coordinate(s) was(were) removed, reverted to a minimum with the symmetry group C1. In fact, it was observed that those transformations in coordinates led to the establishment of intramolecular hydrogen bonds between hydroxyl groups, which are known to have a stabilizing effect in this kind of structures.[21, 30]

Also listed in Tables A.4, A.5 and A.6 is the Gibbs free energy change for the condensation reactions ($\Delta_{\text{R}}G$) that yield each cluster. A negative value for all clusters indicates that the respective condensation reactions are spontaneous. Furthermore, a normalized value of the Gibbs free energy change ($\Delta_{\text{R}}G/s$) was obtained by dividing by the number of Si atoms (s), an index which can be used to compare the free energy of formation of clusters of different compositions, hence giving an estimate of the most probable types of structures that can result from the condensation reactions.[30] According to these results, overall, the cage structures (Q_3^8) are the most favored for all compositions, whereas for the linear structures the clusters with higher degree of condensation are more preferred, which is in agreement with the results obtained in our previous work for aerogels with 100% TMOS, 100% VTMS and 100% MTMS.[30] This last observation is also related to the existence of hydrogen bonds, which have a stabilizing effect on the clusters, as mentioned above. The most favored cyclic clusters are Q_2^4, followed by $Q_2^2Q_1^3Q_1^1$. The values of $\Delta_{\text{R}}G/s$ follow the same trend for all of the aerogel compositions studied. However, in contrast with the results reported by Borba et al.[30], the values of $\Delta_{\text{R}}G/s$ for cyclic clusters are similar to or even lower than those of linear clusters, suggesting that mixing two precursors of different nature has an effect on the formation of cyclic and linear clusters of the resultant materials.

3.2. Infrared spectra analysis

Having obtained the set of most probable silica clusters for each aerogel composition (TMVT, TMAP and TMG), the theoretical vibrational frequencies of all those species were calculated at the B3LYP/6-311+G(d,p) level of theory. The individual theoretical spectra were then simulated by Lorenztian functions with a full width at half maximum of 40 cm^{-1} to emulate peak broadening. No frequency scaling was applied.

A direct comparison between the experimental and the calculated spectra presents a challenge, since the aerogel material is composed of many different silica primary particles, and so each cluster can have a different contribution to the overall spectra. Therefore, it is more sensible to first obtain an overall theoretical spectra for a given composition, which can then be compared to its experimental counterpart. As such, in this work we employed a quantitative strategy to obtain this theoretical spectra, as opposed to a more qualitative approach undertaken in our previous work.[30] The theoretical spectrum of a material was considered to be a weighted sum of the spectra of the individual silica clusters that have been identified in the previous energetic analysis, according to the equation

$$I_{\mathrm{th},j} = k \sum_{i=1}^{n} x_i I_{\mathrm{th},ij} \tag{1}$$

where $I_{\mathrm{th},j}$ is the spectral intensity at frequency index j, x_i is the weight (percentage) associated with each cluster i, $I_{\mathrm{th},ij}$ is the intensity for cluster i at the frequency j and k is an overall scale factor. The unknown values of x_i and k can then be estimated by a numerical fitting of the theoretical intensities to the experimental values. This can be achieved by minimizing the mean squared deviation (MSD) between both spectra:

$$\begin{aligned}
&\min_{x_i,k} MSD = \frac{1}{m}\sum_{j=1}^{m}(I_{\mathrm{exp},j} - I_{\mathrm{th},j})^2 \\
&\text{subject to :} \\
&\sum_{i=1}^{n} x_i = 1 \\
&0 \leq x_i \leq 1 \\
&k > 0
\end{aligned} \tag{2}$$

The minimization problem was solved in MATLAB® using the nonlinear constrained optimization solver `fmincon`. Only a limited frequency range was considered, viz. the 1500 cm^{-1} to 400 cm^{-1} interval, which is the range corresponding to the most relevant vibrations concerning the chemical nature of the aerogel materials studied here. A global optimization solver (`patternsearch`) was also used afterwards, confirming that the solution found was a global minimum. This numerical approach was also extended to the aerogels synthesized from 100% TMOS and 100% VTMS, whose theoretical calculations had been performed previously[30], in order to draw comparisons between the methods published here and there. The results of this numerical procedure are listed in Table 1. As it can be seen, most of the silica clusters were assigned a coefficient of zero. As such, with this strategy we were able to reduce the initial set of silica clusters to a smaller group of those which are the most representative of the aerogel material in spectroscopic (IR) terms. These clusters are represented in Figure 2.

In the case of the aerogels obtained from pure TMOS the values for the optimized fractions of each cluster suggest that cage ($Q_4^3Q_4^2$ and Q_8^3) and cyclic ($Q_2^2Q_1^3Q_1^1$ and $Q_2^3Q_2^2$) clusters provide the best description of the experimental spectrum, as they account for the largest contributions in the model. This is consistent to what was also concluded (albeit by a different approach) in the previous publication.[30] The same is true for VTMS-based clusters, where it was previously concluded (like here) that cage, cyclic and linear structures all have significant contributions to the overall vibrational

spectra, although we have narrowed such contributions to the clusters of type $Q_8^3, Q_3^2, Q_2^3Q_2^2$ and $Q_3^1Q_1^3$, respectively. The silica clusters of the mixture TMVT appear to follow the same trend as that of the pure VTMS-based material, with significant contributions from cage (Q_8^3), cyclic ($Q_2^2Q_1^3Q_1^1$) and linear ($Q_2^3Q_2^2Q_4^1$) structures. These results are consistent with the energetic analysis (Table A.1), as these three clusters exhibited the highest absolute values of $\Delta_{\mathrm{R}}G/s$ among all TMVT clusters, although it should be pointed out that there is no quantitative correlation between these values and those of x_i. In fact, such correlations between $\Delta_{\mathrm{R}}G/s$ and x_i would be very difficult to extract with this model since the numerical fitting procedure is affected by errors in the estimation of the spectral intensities from the DFT calculations, as well as by errors in estimating the peak width, which in experimental conditions is dependent on several factors that cannot be captured by simulating isolated species in vacuum. For the aerogels synthesized from the mixtures TMAP and TMG, cyclic and linear clusters have been identified as the most representative for modeling the aerogel IR spectrum. Again there is no quantitative relationship with the results from the energetic analysis, but in this case the structure that should be the most favored energetically – Q_8^3 – is not part of the numerical spectral model. This result should be viewed in the light of limitations of the model, as discussed above, but also as a possible effect of bulky aminopropyl groups in APTES and glycidylpropoxy groups in GLYMO on the mechanism of formation of the cage clusters. Further studies, possibly with (hugely computationally demanding) *ab initio* molecular dynamics simulations, would answer this question. In spite of the limitations discussed above, this model is still useful to provide a semi-quantitative approximation to the aerogel composition that can be used to represent and study the material at larger scales by means of classical molecular dynamics simulations.

The calculated optimized theoretical spectra and the respective experimental spectra in the frequency ranges of interest can be observed in Figure 3 for the aerogels derived from the precursors TMOS, VTMS, TMVT mixture, TMAP mixture, and TMG mixture. The theoretical spectra for the latter three cases were deconvoluted in order to simplify the vibrational mode analysis, using Lorentzian functions and the Levenberg-Marquardt algorithm for numerical fitting. The assignment of the peak frequencies to vibration modes, according to the literature information and to the modes calculated in the vibration analysis, is also shown in Tables A.7, A.8, and Tables 2 to 4, in the same order. The original experimental spectra for the full frequency range can be viewed in figures A.4 to A.8. Despite the fact that the full spectra, the region 4000–3000 cm^{-1} may contain silanol vibrations of interest, such as those due to the predicted intramolecular hydrogen bonds, these will be masked by the intermolecular hydrogen bonds which cannot be predicted by simulating isolated molecules, and so the analysis of vibration modes will be restricted to the frequency range used for the numerical procedure (see Table 1).

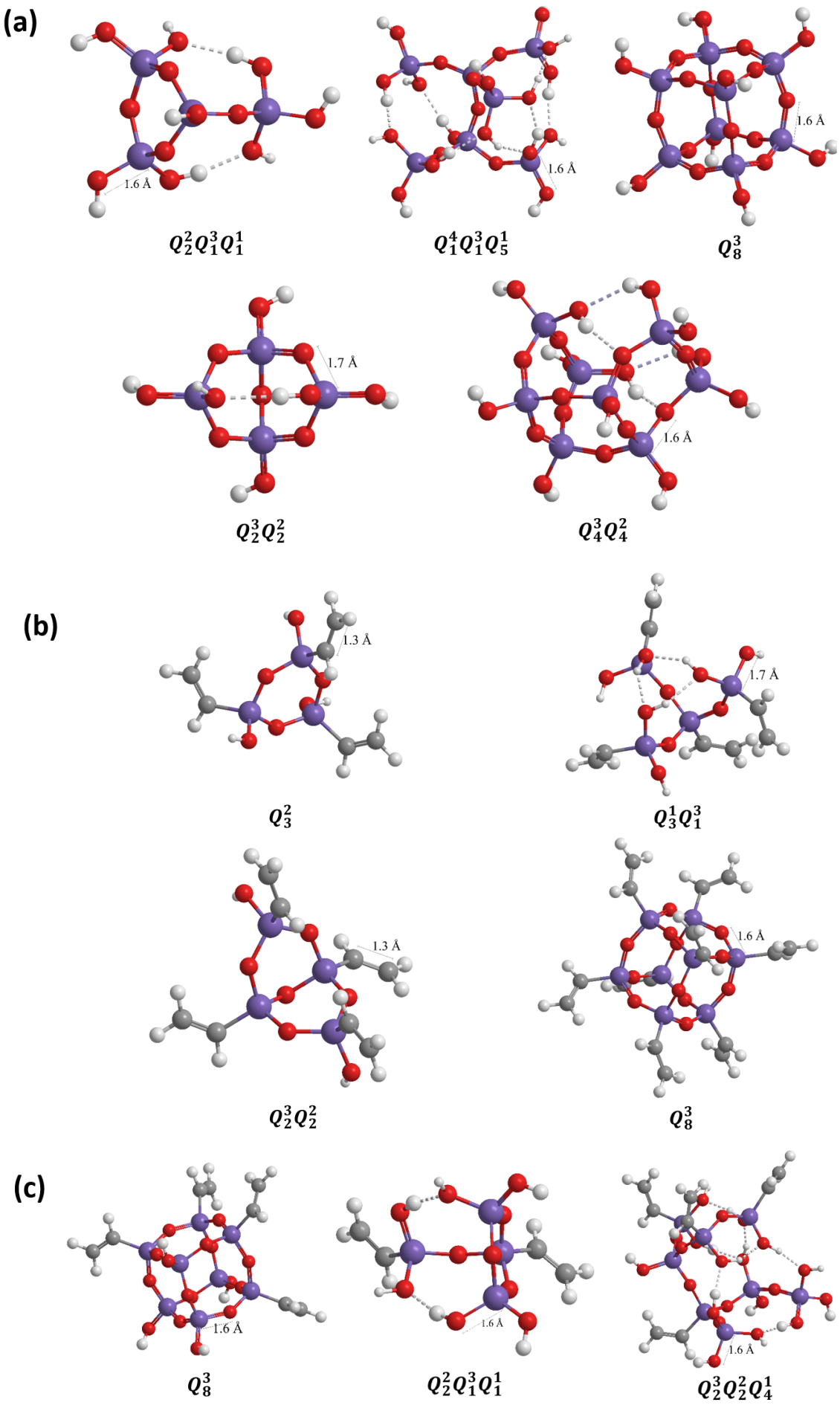

Figure 2: B3LYP/6-311+G(d,p) optimized geometries of the most representative silica clusters, according to Table 1, of the aerogels based on (a) TMOS, (b) VTMS, (c) TMVT, (d) TMAP and (e) TMG. Si atoms in purple, O in red, N in blue, C in grey and H in white. The length of one bond was added for scale. Dashed lines represent hydrogen bonds.

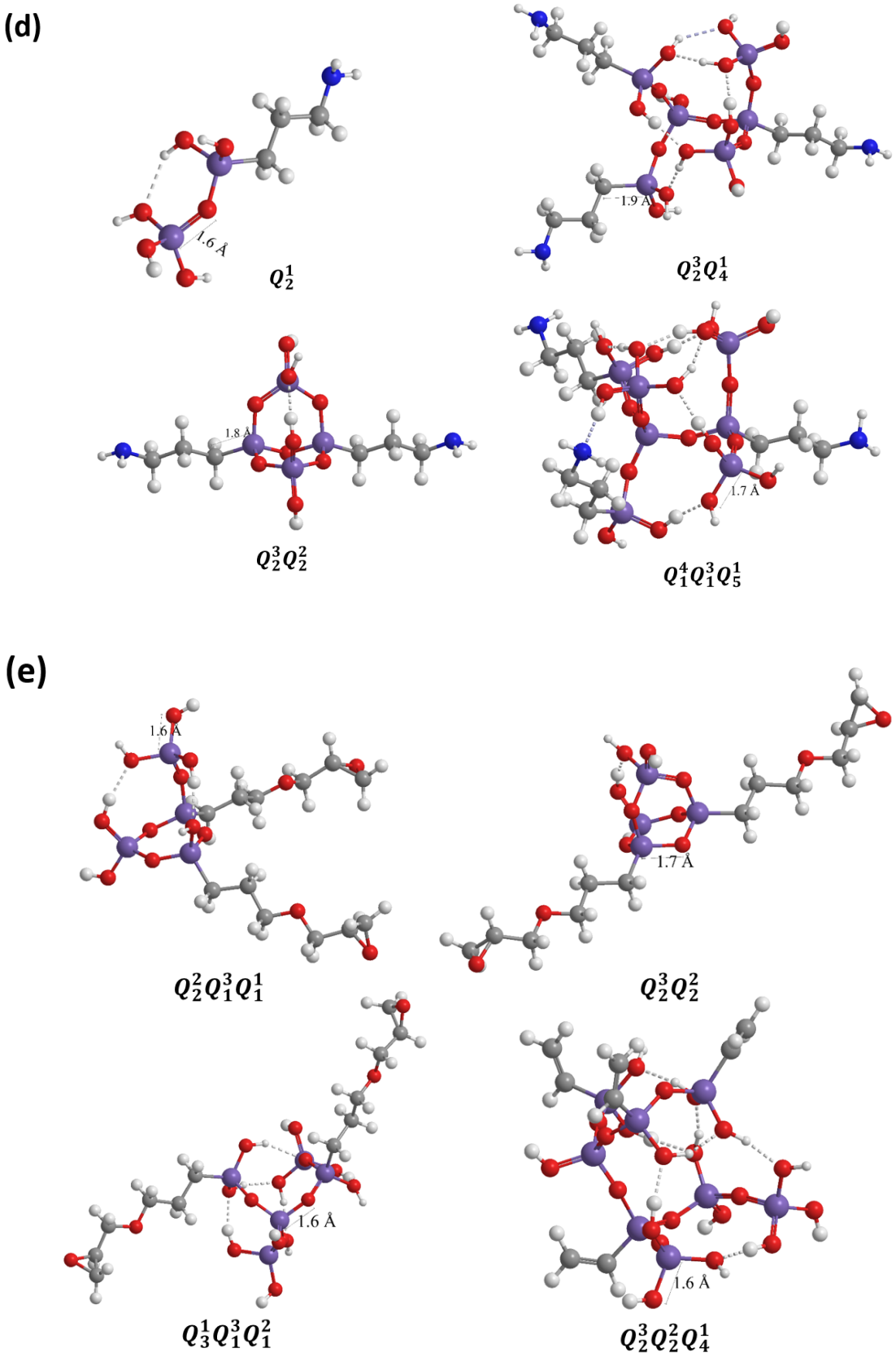

Figure 2 (cont.): B3LYP/6-311+G(d,p) optimized geometries of the most representative silica clusters, according to Table 1, of the aerogels based on (a) TMOS, (b) VTMS, (c) TMVT, (d) TMAP and (e) TMG. Si atoms in purple, O in red, N in blue, C in grey and H in white. The length of one bond was added for scale. Dashed lines represent hydrogen bonds.

Table 1: Results of the numerical optimization of the theoretical spectra in MATLAB®.

Aerogel composition			**TMOS 100%**	**VTMS 100%**	**TMOS 50% VTMS 50%**	**TEOS 50% APTES 50%**	**TEOS 50% GLYMO 50%**
Frequency range used for optimization			400 - 1500 cm^{-1}	400 - 1400 cm^{-1}	400 - 1400 cm^{-1}	500 - 1250 cm^{-1}	500 - 1250 cm^{-1}
$k \times 10^3$			0.323	0.616	0.251	0.138	0.068
x_i	**Cage**	$\mathbf{Q_8^3}$	0.054	0.265	0.262	0.000	0.000
		$\mathbf{Q_4^3Q_4^2}$	0.385	0.000	-	-	-
	Cyclic	$\mathbf{Q_3^2}$	0.000	0.246	0.000	0.000	0.000
		$\mathbf{Q_4^2}$	0.000	0.000	0.000	0.000	0.000
		$\mathbf{Q_2^2Q_1^3Q_1^1}$	0.371	0.000	0.592	0.000	0.277
		$\mathbf{Q_2^3Q_2^2}$	0.081	0.211	0.000	0.485	0.384
		$\mathbf{Q_1^4Q_2^3Q_4^1}$	0.000	-	-	-	-
	Linear	$\mathbf{Q_2^1}$	0.000	0.000	0.000	0.295	0.000
		$\mathbf{Q_2^1Q_1^2}$	0.000	0.000	-	-	-
		$\mathbf{Q_3^1Q_1^3}$	0.000	0.279	-	-	-
		$\mathbf{Q_2^2Q_2^1}$	0.000	0.000	0.000	0.000	0.000
		$\mathbf{Q_3^1Q_1^3Q_1^2}$	0.000	0.000	0.000	0.000	0.225
		$\mathbf{Q_2^3Q_4^1}$	0.000	0.000	0.000	0.033	0.000
		$\mathbf{Q_1^4Q_1^3Q_5^1}$	0.109	-	0.000	0.188	0.000
		$\mathbf{Q_2^3Q_2^2Q_4^1}$	0.000	0.000	0.146	0.000	0.114
Minimum MSD $\times 10^3$			7.228	11.833	2.605	0.237	0.044

The experimental spectra for the TMOS-based aerogel (Figure 3-(a)) is well reproduced by the fitted theoretical counterpart, featuring all of the major peaks of the former. The frequencies of the assigned vibrational modes are all very close to the experimental values (Table A.7), without the need to employ frequency corrections, that are typically required in this type of calculations. This validates the theoretical model proposed in Table 1 for this material. Both spectra are dominated by the two asymmetric Si-O-Si stretching vibration peaks at 1200–1130 cm^{-1} and 1090–1010 cm^{-1}. The former is due to the presence of cage structures (in this case $Q_4^3Q_4^2$ and Q_8^3), and also cage-like structures which are formed from intramolecular hydrogen bonds[30], while the latter is due to linear and cyclic species that do not present such a high degree of condensation or intramolecular hydrogen bonding.

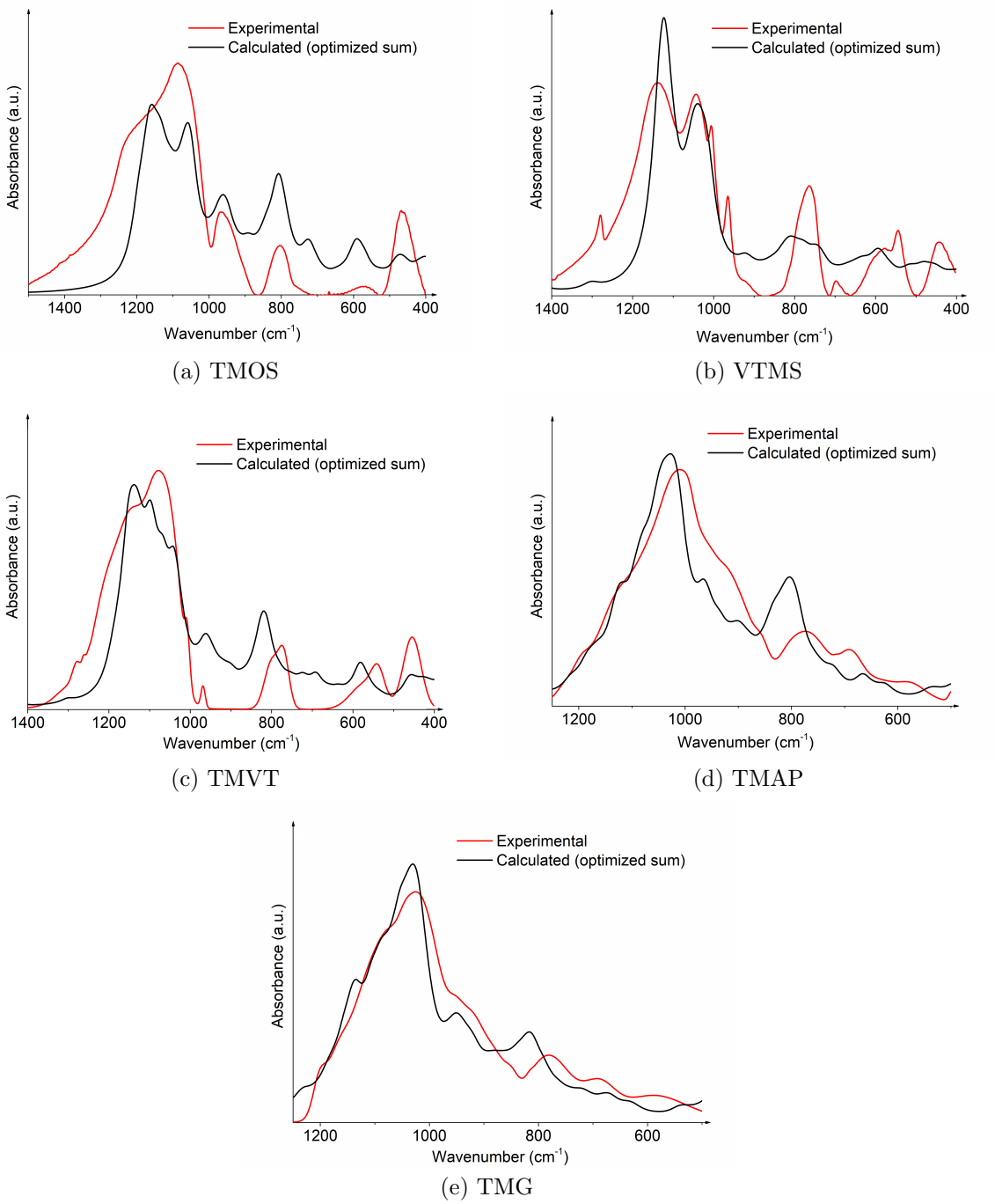

Figure 3: Experimental and theoretical IR spectra for the aerogel based on the indicated precursors.

The same conclusions arise from the vibrational analysis of the VTMS-based aerogel (see Figure 3-(b) and Table A.8), with a very good agreement between experimental and theoretical frequencies for the main peaks (1200–1000 cm^{-1}), although for lower and higher frequencies some deviations are observed. This was also verified in the previous publication for this material.[30] The intensities of the δ(-CH=CH_2) and w(H-C-H) vibration modes of the vinyl groups are not correctly predicted as they are absent in the theoretical spectra, even though these modes are correctly predicted by the DFT calculations. Again, as previously discussed, this is an inherent limitation of the theoretical calculations of the IR spectral intensities.

In the case of the aerogel synthesized from the mixture TMVT (50% TMOS/50% VTMS) the numerical procedure also yields a theoretical spectrum that, overall, matches the experimental one (Figure 3-(c)), and so the major vibrational modes of the siloxane, silanol and vinyl groups in the region 1400–400 cm^{-1} can be reliably identified. The frequencies of the vibration modes, obtained by deconvolution for both experimental and theoretical spectra, match each other well in the region 1200–950 cm^{-1} (Table 2) corresponding to the v_{as}(Si-O-Si) vibration modes, which is to be expected given that the spectral data used for the numerical procedure is dominated by these peaks. However, some deviations occur outside this region, particularly for the δ(=C-H) (1280 cm^{-1}), v(Si-C) (770 cm^{-1}) and v(Si-O)/δ(O-H) (570 cm^{-1}) vibration modes. This kind of deviations are also observed for the frequencies predicted in the case of the VTMS-based aerogel (Table 6), and so were expected here as well.

Finally, for the silica aerogels derived from the mixtures TMAP and TMG (Figures 3-(d) and (e), respectively), the theoretical spectra reproduces the major features of their experimental counterparts, particularly the shape of the v_{as}(Si-O-Si) peaks. It should be noted in the experimental spectra of both materials that the peak ascribed to cage and polycyclic structures (i.e. in the interval 1200–1130 cm^{-1}) appears as a weak shoulder of other v_{as}(Si-O-Si) peak. This may explain why the numerical procedure does not identify the species Q_8^3, and places more emphasis on linear and cyclic clusters with less intramolecular hydrogen bonding ($Q_2^2Q_1^3Q_1^1$, $Q_2^3Q_2^2$ and Q_2^1) associated with the second peak, as discussed previously. This can therefore be indicative that the aminopropyl and gycidylpropoxy groups of APTES and GLYMO have an impact on the formation of cage clusters due to their bulky nature, since the spectra of TMOS, VTMS and TMVT-based aerogels (whose precursors do not have such bulky groups) give strong evidences for the presence of cage and cage-like clusters. The remaining vibration modes that can be attributed to the siloxane, silanol and aminopropyl (for TMAP mixtures) or glycidylpropoxy groups are correctly predicted by the DFT calculations (see tables 3 and 4), and the respective frequencies are generally close to the experimental equivalents (as obtained from the deconvolutions), even though the intensity of the bands is not always predicted correctly. Therefore, these results can confirm the adequacy of the model proposed in table 1 to describe aerogels of TMAP and TMG mixtures.

Table 2: Vibration mode frequency assignment for the deconvoluted experimental and theoretical IR spectra of the 50% TMOS/50% VTMS system, in the region 1400 - 400 cm^{-1}.

Vibration mode [a]	Wavenumber (cm^{-1})		
	Literature [b]	Experimental	Theoretical (optimized sum)
δ(=C-H)	1330 - 1240	1285 1281 1263	1304
v_{as}(Si-O-Si) polycyclic [c]	1200 - 1100	1212 1148	1184 1152 1131 1097
v_{as}(Si-O-Si) cyclic trimers and linear chains	1090 - 1010	1076	1068
δ(O-H)	1040 - 1020	1052 1030	1039
δ(-C**H**=C$\mathbf{H}_2$)	1010 - 990	1007	1039
v(Si-OH) + δ(O-H) *in-plane*	955 - 830	969	960 909
v(Si-C)	785 - 805	797 797[d]	819 757
v_s(Si-O-Si)	800 - 680	769	723 691
v(Si-O)	580 - 550	569	641
δ(O-H) *out-of-plane*	710 - 570		581
γ(=C-H)	530 - 540	538	547
δ(O-Si-O) *in-plane*	459 - 469	454	460
δ(O-Si-O) δ(Si-C=C) *in-plane*		-	415

[a] v - stretching; v_s - symmetric stretching; v_{as} - asymmetric stretching; δ - bending. [b] Refs [38, 39]. [c] Includes species with intramolecular hydrogen bonds that form polycyclic-like structures. [d] Possible overlap

3.3. NMR spectra analysis

In order to complement the IR spectra analysis and further validate the theoretical model of the silica aerogel materials here obtained, solid-state ^{29}Si-NMR-MAS measurements have been performed, whose resulting spectra are shown in figure 4. In addition, the ^{29}Si NMR chemical shifts of the most stable silica clusters for each material were estimated by DFT calculations with the GIAO method and the IGLO-III basis set. The theoretical and experimental chemical shifts can be compared in tables A.9 and A.10 (S.I.), for TMOS and VTMS-based aerogels, and tables 5, and 6 7 for the remaining materials. For all clusters a systematic overestimation of the chemical shifts are observed, which can be attributed to errors inherent to the calculation (typical deviations can go up to 12 ppm)[40]. The peaks of the ^{29}Si-NMR spectra are assigned to the different chemical environments of the Si atoms according to the "Q" notation, already used in our previous publication, where tetrafunctional (Qx)

Table 3: Vibration mode frequency assignment for the deconvoluted experimental and theoretical IR spectra of the 50% TEOS/50% APTES system, in the region 1250 - 500 cm^{-1}.

Vibration mode [a]	Wavenumber (cm^{-1})		
	Literature [b]	Experimental	Theoretical (optimized sum)
$w(CH_2)$	1250 - 1280	1228	1218
$\gamma(NH_2)$	1295 - 1145	[d]	[e]
v_{as}(Si-O-Si) polycyclic [c]	1200 - 1100	1197	1176
		1118	1126
$v(C\text{-}NH_2)$	1090 - 1020	1085[d]	1083[e]
v_{as}(Si-O-Si) cyclic trimers and linear chains	1090 - 1010	1085	1083
		1059	1049
δ(O-H)	1040 - 1020	1034	1025
		1007	1012
$v(CH_2\text{-}CH_2)$		1034[d]	1025
$\gamma(CH_2)$		1007[d]	1012
		993	963
v(Si-O) + δ(O-H)	955 - 830	956	963
		921	936
		882	898
		855	833
		813	
$v(Si\text{-}CH_2)$	810 - 800		833
v_s(Si-O-Si)	800 - 680	770	799
$w(\text{-}NH_2)$	895 - 650		751
$r(\text{-}CH_2\text{-})$	760 - 670	688	722
v_s(Si-O-Si)	800 - 680		665
v_s(Si-O-Si)	800 - 680	637	625
v(Si-O)	580 - 550	575	537
δ(O-H) *out-of-plane*	710 - 570		
δ(O-Si-O)			
$\delta(\mathbf{C}H_2\text{-}\mathbf{C}H_2\text{-}\mathbf{C}H_2)$	495 - 445	495	491
$\delta(\mathbf{C}H_2\text{-}\mathbf{C}H_2\text{-}\mathbf{N}H_2)$			

[a] v - stretching; v_s - symmetric stretching; v_{as} - asymmetric stretching; δ - bending. [b] Refs [38, 39]. [c] Includes species with intramolecular hydrogen bonds that form polycyclic-like structures. [d] Possibly overlapped with the v_{as} (Si-O-Si) peaks. [e] These vibrations are present in the theoretical spectra but have very low intensity and are hidden in larger neighbouring peaks.

and trifunctional (Tx) Si atoms (the latter incorporating one functional group that cannot undergo hydrolysis) are classified according to the degree of condensation (x is the number of Si atoms that are linked to the Si atom in question by Si-O-Si bridges)[30].

As Figure 4-(a) shows, three peaks are identified the ^{29}Si-NMR spectrum of the TMOS aerogel, corresponding, in decreasing order of intensity, to Si atoms in the Q4, Q3 and Q2 environments (see

Table 4: Vibration mode frequency assignment for the deconvoluted experimental and theoretical IR spectra of the 50% TEOS/50% GLYMO system, in the region 1250 - 500 cm^{-1}.

Vibration mode [a]	Wavenumber (cm^{-1})		
	Literature [b]	Experimental	Theoretical (optimized sum)
w(-CH_2-), γ(CH_2)	1250 - 1280	-	1233
δ(-CH_2-(O)-CH-)	1210 - 1140	1202	1137
v_{as}(CH_2-O-CH_2)	1150 - 1060	1170[d]	
v_{as}(Si-O-Si) polycyclic [c]	1200 - 1100	1170	1182
		1110	1157
			1108
v_{as}(Si-O-Si) cyclic trimers and linear chains	1090 - 1010	1078	1088
		1047	1054
δ(O-H)	1040 - 1020	1021	1027
v_s(CH_2-O-CH_2)	1140 - 820	1021[d]	1013
v(CH_2-CH_2), γ(CH_2)			
v(Si-O) + δ(O-H)	955 - 830	952	950
		922	922
v(Si-O) + δ(O-H)	955 - 830	880	876
v_{as}(-CH_2-(O)-CH-)	880 - 775	849	
v(Si-O) + δ(O-H)	955 - 830	817	815
v_s(Si-O-Si)	800 - 680	783	761
v(Si-CH_2)	810 - 800		
r(-CH_2-)	760 - 670	753	719
			672
v_s(Si-O-Si)	800 - 680	689	630
δ(SiO-H) *out-of-plane*	710 - 570		
δ(O-H) *out-of-plane*			538
δ(O-Si-O)		586	
δ(**C**H_2-**C**H_2-**C**H_2)	540 - 485		486
δ(**C**H_2-**C**H_2-**O**-)			

[a] v - stretching; v_s - symmetric stretching; v_{as} - asymmetric stretching; δ - bending. [b] Refs [38, 39]. [c] Includes species with intramolecular hydrogen bonds that form polycyclic-like structures. [d] Possibly overlapped with the v_{as} (Si-O-Si) peaks.

assignments in Table A.9). These observations indicate the presence of clusters with a high degree of condensation, a feature that is line with the conclusion derived from the IR spectra analysis, according to which cage and cyclic clusters are the most representative structures of the TMOS-based aerogel. In fact all the species identified in Table 1 possess the chemical environments (Q4, Q3 and Q2) that are associated with the spectrum of Figure 4-(a), thus confirming as well the validity of the model presented herein. Similarly, for the VTMS-based aerogel (Figure 4-(b) and Table A.10), the peaks identified in the ^{29}Si-NMR spectrum correspond to T3 and T2 environments, which are present in the Q_8^3, Q_3^2, $Q_2^3Q_2^2$ and $Q_3^1Q_1^3$ clusters, a result which also substantiates the numerical model. On the

other hand, the Q1 peaks cannot be identified in Figure 4-(a), and the same applies to the T1 peaks in Figure 4-(b), probably because they have very low intensity and cannot be distinguished from the signal noise.

The results of the ^{29}Si-NMR analysis for the TMAP-based aerogels (Figure 4-(d) and Table 6) also seem to support the numerical model derived from the IR spectra analysis. In fact, the chemical environments present in the ^{29}Si-NMR spectra (Q4,Q3,Q2,T3,T2 and T1) are accounted for in the clusters identified in the model ($Q_2^3Q_2^2$, Q_2^1, $Q_2^3Q_4^1$, and $Q_1^4Q_1^3Q_5^1$), Furthermore, the relatively weaker intensity of the Q3 peak in the ^{29}Si-NMR spectra is consistent with the evidence exhibited in the IR spectra for the absence of cage-like clusters (when compared, for instance, to the spectrum of the TMVT-based aerogel in figure 4-(c), a material which was demonstrated to feature cage structures),

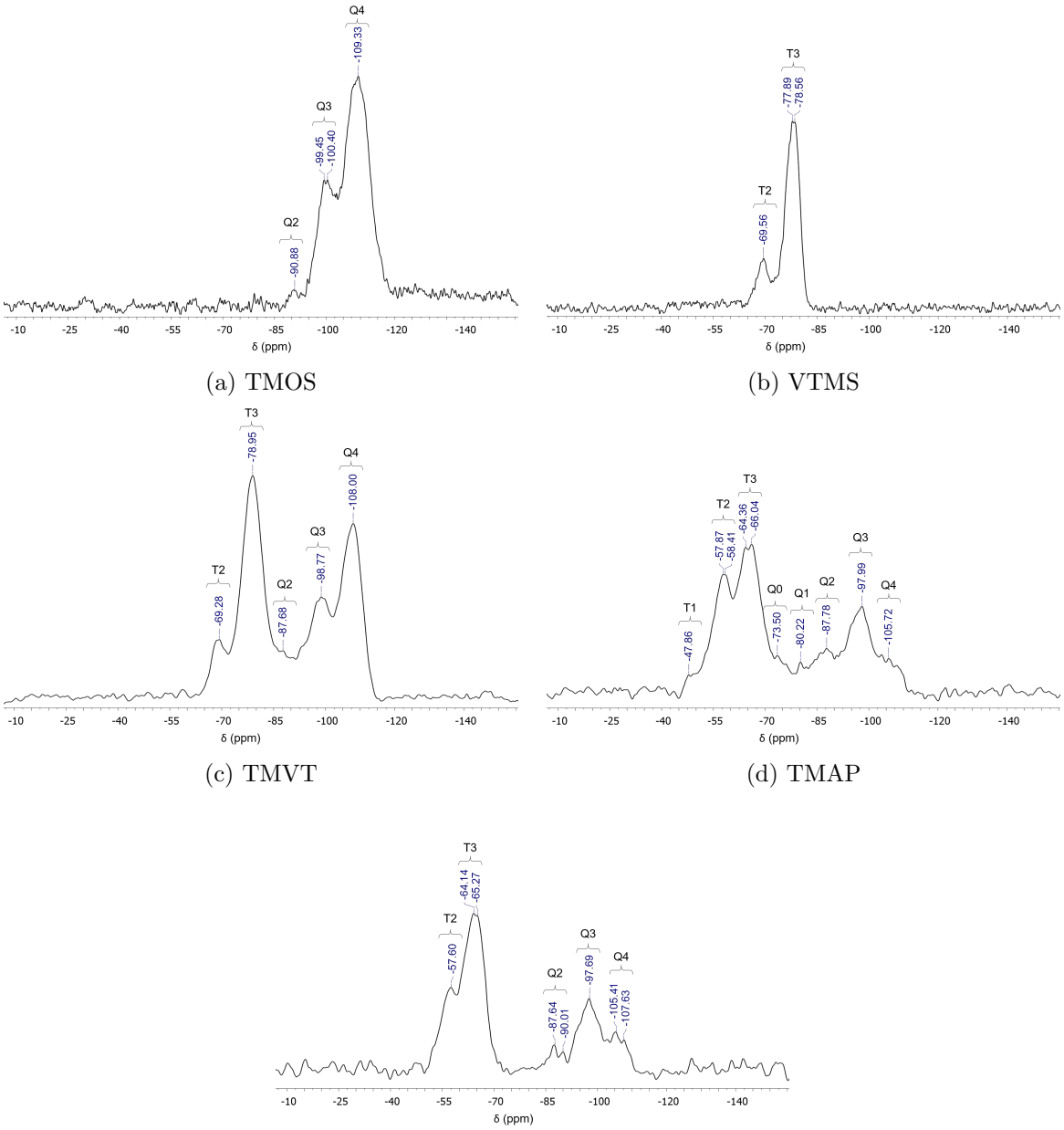

(a) TMOS (b) VTMS

(c) TMVT (d) TMAP

(e) TMG

Figure 4: Solid-state ^{29}Si-NMR-MAS of the aerogel derived from TMOS. Chemical shifts (in ppm) relative to TMS. The spectra of figures (c), (d) and (e) were smoothed with an exponential apodization at 120 Hz in order to improve the signal to noise ratio.

and as such the Q3 peak can be related to other species ($Q_2^3Q_2^2$, $Q_2^3Q_4^1$, and $Q_1^4Q_1^3Q_5^1$).

This analysis is not so conclusive for the aerogels of the mixtures TMVT and TMG (Figures 4-(c) and 4-(e) and Tables 5 and 7, respectively). While the majority of the Si chemical environments revealed by the ^{29}Si-NMR spectra (namely Q3, Q2, T3 and T2) are also present in the most representative clusters identified in Table 1 (TMVT: Q_8^3, $Q_2^2Q_1^3Q_1^1$ and $Q_2^3Q_2^2Q_4^1$; TMG: $Q_2^2Q_1^3Q_1^1$, $Q_2^3Q_2^2$, $Q_3^1Q_1^3Q_1^2$, and $Q_2^3Q_2^2Q_4^1$), there is a significant peak corresponding to the Q4 environment in the ^{29}Si-NMR spectra of these materials which is not accounted for in the case of the theoretical approach. The silica cluster studied in this work that has such an environment – $Q_1^4Q_1^3Q_5^1$ – has a coefficient of 0 in the spectral numerical model. However, it should be noted that this does not completely invalidate the latter, as the Q4 environment may also be due to condensation reactions between the silica clusters, which happen in a scale beyond the scope of the model (i.e. above supramolecular scale). Hybrid quantum mechanics/molecular mechanics (QM/MM) simulations, with the QM part of the system focused on the reactions between hydroxyl groups of aggregated silica primary particles, may help in clarifying this question.

4. Conclusion

ORMOSIL aerogels of three different mixtures of precursors – 50% TMOS/50% VTMS (TMVT), 50% TEOS/50% APTES (TMAP) and 50% TEOS/50% GLYMO (TMG) – have been studied by DFT calculations. Several conformers of different types of silica clusters, having cage, cyclic and linear structures, were analyzed at the B3LYP/6-311+G(d,p) level of theory. The resulting thermochemical data, in particular the Gibbs free energy, allowed the identification of the most stable conformers for each type of cluster. Furthermore, the normalized value of the Gibbs free energy change of the condensation reaction responsible for the formation of each cluster ($\Delta_{\mathrm{R}}G/s$) permitted a comparison between different types of structures, from which it was concluded that cage specimens were the most favored, followed by cyclic and linear clusters with high degrees of condensation.

Vibrational frequencies of each silica cluster were also computed at the same level of theory, thus providing a theoretical spectra to be compared with the experimental counterpart. This was achieved by a numerical model in which the overall theoretical spectrum was considered as a weighted sum of individual theoretical spectrum of each silica cluster, with the weights being optimized using nonlinear optimization. Overall, the theoretical spectra obtained in this fashion were able to reproduce well their experimental counterparts, allowing the identification of the main vibration modes in the frequency region allocated to the numerical analysis. The calculated frequencies of the vibration modes were close to the experimental values, especially for the peak corresponding to the v_{as}(Si-O-Si) mode, which has the highest intensity, although the spectral intensities were not always matched. This analysis was also extended and successfully applied to the aerogels derived from pure TMOS and pure VTMS, whose calculations were already performed in a previous work but analyzed by means of a different approach.

Furthermore, an analysis of ^{29}Si-NMR experimental spectra, combined with theoretical chemical shift predictions with the GIAO method at the B3LYP/IGLO-III level of theory, provided further data to support the spectroscopic model derived numerically. For the aerogel materials of 100% TMOS, 100% VTMS and 50% TEOS/50% APTES the observed ^{29}Si-NMR peaks matched those expected for

the set of most probable silica cluster identified in the numerical model. However, for the aerogels obtained from the TMVT and TMG mixtures of precursors, the model failed to explain the existence of the Q4 peak, although it should be pointed out that the ^{29}Si-NMR spectra also has contributions from species at a higher scale than those studied herein.

In summary, this work provided new insights into the targeted silica aerogel compositions by allowing the identification of the most probable constitutive silica clusters. Furthermore, it provided crucial data towards establishing a multiscale molecular modeling and simulation approach for the study of the title silica aerogels.

Acknowledgments

Funding: this work was developed as part of the project AerogelDustFree - Aerogel for Space applications ISO8 without dust release (Contract No. 17815), developed by the consortium Active Aerogels / University of Coimbra, funded by the European Regional Development Fund (FEDER) through the Regional Operational Program of the Center of Portugal (Centro2020) of PT2020. The authors wish to thank to João Vareda from the Department of Chemical Engineering, University of Coimbra, and to Marta Ochoa and Inês Rocha from ACTIVE AEROGELS, Coimbra, for providing experimental data.

Table 5: Experimental ^{29}Si-NMR chemical shifts, respective Si environments denoted by the Qx notation (see main text), and theoretically calculated values for all silica clusters of the aerogel synthesized from the TMVT mixture.

Species		Chemical shifts for different Si environments (ppm) [a]								
		Q4	Q3	Q2	Q1	Q0	T3	T2	T1	T0
Theoretical	Q_8^3	N/A	-114.28 to -115.31	N/A	N/A	N/A	-91.74 to -93.16	N/A	N/A	N/A
	Q_3^2	N/A	N/A	-95.83 -96.16	N/A	N/A	N/A	-73.52	N/A	N/A
	Q_4^2	N/A	N/A	-99.71 -101.05	N/A	N/A	N/A	-75.01 -76.73	N/A	N/A
	$Q_2^2Q_1^3Q_1^1$	N/A	N/A	-93.01 -95.25	N/A	N/A	-79.30	N/A	-69.97	N/A
	$Q_2^3Q_2^2$	N/A	-96.18	-93.02	N/A	N/A	-69.49	-70.67	N/A	N/A
	Q_2^1	N/A	N/A	N/A	-86.05	N/A	N/A	N/A	-66.27	N/A
	$Q_2^1Q_2^1$	N/A	N/A	-98.38	-91.09	N/A	N/A	-79.15	-65.20	N/A
	$Q_3^1Q_1^3Q_1^2$	N/A	-119.66	-107.14	-91.32	N/A	N/A	N/A	-70.76 -72.53	N/A
	$Q_2^3Q_4^1$	N/A	-113.43 -113.53	N/A	-92.50	N/A	N/A	N/A	-62.18 to -68.59	N/A
	$Q_1^4Q_1^3Q_5^1$	-124.58	-113.12	N/A	-90.55 -97.23	N/A	N/A	N/A	-62.97 to -72.10	N/A
	$Q_2^3Q_2^2Q_4^1$	N/A	-122.88	-107.74	-96.00 -96.91	N/A	-98.63	-74.86	-67.00 -71.79	N/A
	TMOS	N/A	N/A	N/A	N/A	-81.11	N/A	N/A	N/A	N/A
	VTMS	N/A	N/A	N/A	N/A	N/A	N/A	N/A	N/A	-59.48
Experimental		-108.00	-98.77	-87.68	Overlap with T3	Overlap with T2	-79.95	-69.28	Not observed	Not observed
Literature [b]		-120 to -104	-104 to -94	-96 to -85	-85 a -75	-75 to -66	-81 to -76	-72 to -66	-63 to -59	-59 to -50

[a] Chemical shifts relative to tetramethylsilane (TMS). In the case of the theoretical spectra, δ_{Si} (TMS) = 330.18 ppm. [b] Refs [30, 41, 42]

Table 6: Experimental ^{29}Si-NMR chemical shift assignments to Si environments denoted by the Qx notation (see main text), and theoretically calculated values for all silica clusters of the aerogel obtained from the TMAP mixture of precursors.

Species		Chemical shifts for different Si environments (ppm) [a]								
		Q4	Q3	Q2	Q1	Q0	T3	T2	T1	T0
Theoretical	Q_8^3	N/A	-114.82 to -115.21	N/A	N/A	N/A	-75.08 to -77.57	N/A	N/A	N/A
	Q_3^2	N/A	N/A	-95.75 -96.20	N/A	N/A	N/A	-60.66	N/A	N/A
	Q_4^2	N/A	N/A	-104.87 -106.12	N/A	N/A	N/A	-66.20 -67.32	N/A	N/A
	$Q_2^2Q_1^3Q_1^1$	N/A	N/A	N/A	-90.91 -94.41	N/A	-63.15	-52.36	N/A	N/A
	$Q_2^3Q_2^2$	N/A	N/A	-93.18 -93.59	N/A	N/A	-52.57 -52.49	N/A	N/A	N/A
	Q_2^1	N/A	N/A	N/A	-90.84	N/A	N/A	N/A	-51.00	N/A
	$Q_2^1Q_2^1$	N/A	N/A	N/A	-90.77	N/A	N/A	-63.70	N/A	N/A
	$Q_3^1Q_1^3Q_1^2$	N/A	-114.62	N/A	-91.69 -94.07	N/A	N/A	-59.60	-49.53	N/A
	$Q_2^3Q_4^1$	N/A	-121.77	N/A	-90.18 -90.64	N/A	-79.15	N/A	-57.31	N/A
	$Q_1^4Q_1^3Q_5^1$	-130.04	N/A	N/A	-94.71 to -96.84	N/A	-81.36	N/A	-57.42 -58.06	N/A
	$Q_2^3Q_2^2Q_4^1$	N/A	N/A	-100.63 -102.03	-95.15 -95.61	N/A	-83.32 -85.86	N/A	-49.62 -49.90	N/A
	TMOS	N/A	N/A	N/A	N/A	-81.11	N/A	N/A	N/A	N/A
	APTMS	N/A	N/A	N/A	N/A	N/A	N/A	N/A	N/A	-42.28
Experimental		-105.72	-97.99	-87.78	-80.22	-73.50	-64.36 -66.04	-57.87 -58.41	-47.86	Not observed
Literature [b]		-120 to -104	-104 to -94	-96 to -85	-85 a -75	-75 to -66	-70 to -61 [c]	-61 to -52 [c]	-52 to -47 [c]	-40 to -47 [c]

[a] Chemical shifts relative to tetramethylsilane (TMS). In the case of the theoretical spectra, δ_{Si} (TMS) = 330.18 ppm. [b] Refs [30, 41–43]. [c] These values correspond to aerogels synthesized from the precursor 1,6-bis(trimethoxysilyl)hexane ($(MeO)_3$-Si-$(CH_2)_6$-Si-$(OMe)_3$) and as such, given that the Si atom in APTMS ($(MeO)_3$-Si-$(CH_2)_3$-NH_2) has a similar chemical environment than in that precursor, we assume that the chemical shifts T3 a T0 will be applicable in this case.

Table 7: Experimental ^{29}Si-NMR chemical shift assignments to Si environments denoted by the Qx notation, and theoretically calculated values for all silica clusters of the aerogel synthesized from the TMG mixture.

Species		Chemical shifts for different Si environments (ppm) [a]								
		Q4	Q3	Q2	Q1	Q0	T3	T2	T1	T0
Theoretical	Q_8^3	N/A	-114.97 to -115.62	N/A	N/A	N/A	-75.72 to -78.19	N/A	N/A	N/A
	Q_3^2	N/A	N/A	-95.84 -96.50	N/A	N/A	N/A	-57.41	N/A	N/A
	Q_4^2	N/A	N/A	-95.40	N/A	N/A	N/A	-55.17	N/A	N/A
	$Q_2^2Q_1^3Q_1^1$	N/A	N/A	-94.43	-91.14	N/A	-63.53	-52.54	N/A	N/A
	$Q_2^3Q_2^2$	N/A	N/A	-93.28 -93.37	N/A	N/A	-52.16 -52.42	N/A	N/A	N/A
	Q_2^1	N/A	N/A	N/A	-85.34	N/A	N/A	N/A	-46.98	N/A
	$Q_2^1Q_2^1$	N/A	N/A	N/A	-90.57	N/A	N/A	N/A	-63.29	N/A
	$Q_3^1Q_1^3Q_1^2$	N/A	-113.54	N/A	-91.29 -86.64	N/A	N/A	-58.24	-51.84	N/A
	$Q_2^3Q_4^1$	N/A	-117.65	N/A	-92.64 -94.10	N/A	-79.60	N/A	-51.89 -55.42	N/A
	$Q_1^4Q_1^3Q_5^1$	-129.84	N/A	N/A	-90.65 to -95.83	N/A	-80.05	N/A	-53.71 -56.76	N/A
	$Q_2^3Q_2^2Q_4^1$	N/A	-119.46	-106.40	-96.13 -96.59	N/A	-81.40	-58.99	-51.67 -53.76	N/A
	TMOS	N/A	N/A	N/A	N/A	-81.11	N/A	N/A	N/A	N/A
	GLYMO	N/A	N/A	N/A	N/A	N/A	N/A	N/A	N/A	-42.82
Experimental		-105.41 -107.63	-97.69	-87.64 -90.01	Not observed	Overlap with T3	-64.14 -65.27	-57.60	Not observed	Not observed
Literature [b]		-120 to -104	-104 to -94	-96 to -85	-85 to -75	-75 to -66	-70 to -61 [c]	-61 to -52 [c]	-52 to -47 [c]	-40 to -47 [c]

[a] Chemical shifts relative to tetramethylsilane (TMS). In the case of the theoretical spectra, δ_{Si} (TMS) = 330.18 ppm. [b] Refs [30, 41–43]. [c] These values correspond to aerogels synthesized from the precursor 1,6-bis(trimethoxysilyl)hexane ($(MeO)_3$-Si-$(CH_2)_6$-Si-$(OMe)_3$) and as such, given that the Si atom in GLYMO ($(MeO)_3$-Si-$(CH_2)_3$-O-CH_2-(-CH-O-CH_2-)) has a similar chemical environment than in that precursor, we assume that the chemical shifts T3 a T0 will be applicable in this case.

References

[1] S. S. Kistler, Coherent expanded aerogels and jellies, Nature 127 (1931) 741. doi:10.1038/127741a0.

[2] M. Aegerter, N. Leventis, M. Koebel, Aerogels Handbook, Advances in Sol-Gel Derived Materials and Technologies, Springer New York, 2011.

[3] N. Bheekhun, A. R. Abu Talib, M. R. Hassan, Aerogels in aerospace: An overview, Advances in Materials Science and Engineering 2013 (2013) 18. doi:10.1155/2013/406065.

[4] H. Maleki, L. Dures, A. Portugal, An overview on silica aerogels synthesis and different mechanical reinforcing strategies, Journal of Non-Crystalline Solids 385 (2014) 55 – 74. doi:10.1016/j.jnoncrysol.2013.10.017.

[5] J. L. Gurav, I.-K. Jung, H.-H. Park, E. S. Kang, D. Y. Nadargi, Silica aerogel: Synthesis and applications, Journal of Nanomaterials 2010 (2010) 11. doi:10.1155/2010/409310.

[6] Y. N. Kharzheev, Use of silica aerogels in cherenkov counters, Physics of Particles and Nuclei 39 (1) (2008) 107–135. doi:10.1134/S1063779608010085.

[7] J. P. Vareda, A. Lamy-Mendes, L. Dures, A reconsideration on the definition of the term aerogel based on current drying trends, Microporous and Mesoporous Materials 258 (2018) 211 – 216. doi:10.1016/j.micromeso.2017.09.016.

[8] H. H. Tang, E. S. Orndoff, L. A. Trevino, Thermal performance of space suit elements with aerogel insulation for moon and mars exploration, in: SAE Technical Paper, SAE International, 2006. doi:10.4271/2006-01-2235.

[9] A. V. Rao, S. D. Bhagat, H. Hirashima, G. Pajonk, Synthesis of flexible silica aerogels using methyltrimethoxysilane (MTMS) precursor, Journal of Colloid and Interface Science 300 (1) (2006) 279 – 285. doi:10.1016/j.jcis.2006.03.044.

[10] L. Durães, M. Ochoa, A. Portugal, N. Duarte, J. P. Dias, N. Rocha, J. Hernandez, Tailored silica based xerogels and aerogels for insulation in space environments, in: 12th INTERNATIONAL CERAMICS CONGRESS PART B, Vol. 63 of Advances in Science and Technology, Trans Tech Publications, 2011, pp. 41–46. doi:10.4028/www.scientific.net/AST.63.41.

[11] L. Cai, G. Shan, Elastic silica aerogel using methyltrimethoxysilane precusor via ambient pressure drying, Journal of Porous Materials 22 (6) (2015) 1455–1463. doi:10.1007/s10934-015-0026-6.

[12] T. Matias, C. Varino, H. C. de Sousa, M. E. M. Braga, A. Portugal, J. F. J. Coelho, L. Durães, Novel flexible, hybrid aerogels with vinyl- and methyltrimethoxysilane in the underlying silica structure, Journal of Materials Science 51 (14) (2016) 6781–6792. doi:10.1007/s10853-016-9965-9.

[13] S. Cui, B. Lin, Y. Liu, X. Liu, X. Shen, G. Han, X. Zhou, Preparation and adsorption capacity of vinyltriethoxysilane modified silica aerogels, Current Nanoscience 8. doi:10.2174/157341312802884445.

[14] M. A. B. Meador, E. F. Fabrizio, F. Ilhan, A. Dass, G. Zhang, P. Vassilaras, J. C. Johnston, N. Leventis, Cross-linking amine-modified silica aerogels with epoxies: mechanically strong lightweight porous materials, Chemistry of Materials 17 (5) (2005) 1085–1098. doi:10.1021/cm048063u.

[15] U. Schubert, F. Schwertfeger, N. Hsing, E. Seyfried, Inorganic-organic hybrid aerogels, MRS Proceedings 346 (1994) 151. doi:10.1557/PROC-346-151.

[16] P. Rogl, R. Podloucky, W. Wolf, Dft calculations: A powerful tool for materials design, Journal of Phase Equilibria and Diffusion 35 (3) (2014) 221–222. doi:10.1007/s11669-014-0309-7.

[17] M. O. Steinhauser, S. Hiermaier, A review of computational methods in materials science: examples from shock-wave and polymer physics, International journal of molecular sciences 10 (12) (2009) 5135–5216. doi:10.3390/ijms10125135.

[18] X. Cheng, D. Chen, Y. Liu, Mechanisms of silicon alkoxide hydrolysisoligomerization reactions: A DFT investigation, ChemPhysChem 13 (9) (2012) 2392–2404. doi:10.1002/cphc.201200115.

[19] H. Henschel, A. M. Schneider, M. H. Prosenc, Initial steps of the solgel process: Modeling silicate condensation in basic medium, Chemistry of Materials 22 (17) (2010) 5105–5111. doi:10.1021/cm100401f.

[20] X.-Q. Zhang, T. T. Trinh, R. A. van Santen, A. P. J. Jansen, Mechanism of the initial stage of silicate oligomerization, Journal of the American Chemical Society 133 (17) (2011) 6613–6625, pMID: 21486018. doi:10.1021/ja110357k.

[21] T. T. Trinh, A. P. J. Jansen, R. A. van Santen, E. J. Meijer, Role of water in silica oligomerization, The Journal of Physical Chemistry C 113 (7) (2009) 2647–2652. doi:10.1021/jp076372c.

[22] E. Monsivais-Gámez, F. Ruiz, J. R. Martínez, Four-membered rings family in the Si-O extended rocking IR band from quantum chemistry calculations, Journal of Sol-Gel Science and Technology 43 (1) (2007) 65–72. doi:10.1007/s10971-007-1578-y.

[23] A. Depla, D. Lesthaeghe, T. S. van Erp, A. Aerts, K. Houthoofd, F. Fan, C. Li, V. Van Speybroeck, M. Waroquier, C. E. A. Kirschhock, J. A. Martens, ^{29}Si NMR and UV–Raman investigation of initial oligomerization reaction pathways in acid-catalyzed silica solgel chemistry, The Journal of Physical Chemistry C 115 (9) (2011) 3562–3571. doi:10.1021/jp109901v.

[24] P. I. Pohl, J.-L. Faulon, D. M. Smith, Molecular dynamics computer simulations of silica aerogels, Journal of Non-Crystalline Solids 186 (1995) 349 – 355, proceedings of the Fourth International Symposium on AEROGELS. doi:10.1016/0022-3093(95)00042-9.

[25] J. C. G. Pereira, C. R. A. Catlow, G. D. Price, Molecular dynamics simulation of methanolic and ethanolic silica-based solgel solutions at ambient temperature and pressure, The Journal of Physical Chemistry A 106 (1) (2002) 130–148. doi:10.1021/jp010078h.

[26] J. Lei, Z. Liu, J. Yeo, T. Y. Ng, Determination of the young's modulus of silica aerogels an analyticalnumerical approach, Soft Matter 9 (2013) 11367–11373. doi:10.1039/C3SM51926K.

[27] C. A. Ferreiro-Rangel, L. D. Gelb, Investigation of the bulk modulus of silica aerogel using molecular dynamics simulations of a coarse-grained model, The Journal of Physical Chemistry B 117 (23) (2013) 7095–7105, pMID: 23631801. doi:10.1021/jp3128737.

[28] C. A. Ferreiro-Rangel, L. D. Gelb, Computational study of uniaxial deformations in silica aerogel using a coarse-grained model, The Journal of Physical Chemistry B 119 (27) (2015) 8640–8650, pMID: 26039801. doi:10.1021/jp512998w.

[29] A. Borba, M. Almangano, A. A. Portugal, R. Patrcio, P. N. Simes, Methylsilsesquioxane-based aerogel systemsinsights into the role of the formation of molecular clusters, The Journal of Physical Chemistry A 120 (23) (2016) 4079–4088, pMID: 27213224. doi:10.1021/acs.jpca.6b04196.

[30] A. Borba, J. P. Vareda, L. Dures, A. Portugal, P. N. Simes, Spectroscopic characterization of silica aerogels prepared using several precursors effect on the formation of molecular clusters, New J. Chem. 41 (2017) 6742–6759. doi:10.1039/C7NJ01082F.

[31] I. Ospino, A. Luquin, M. Jimnez-Ruiz, J. I. Prez-Landazbal, V. Recarte, J. C. Echeverra, M. Laguna, A. A. Urtasun, J. J. Garrido, Computational modeling and inelastic neutron scattering contributions to the study of methyl-silica xerogels: A combined theoretical and experimental analysis, The Journal of Physical Chemistry C 121 (41) (2017) 22836–22845. doi:10.1021/acs.jpcc.7b07310.

[32] I. Rocha, M. Ochoa, Private Communication, ACTIVE AEROGELS, Parque Industrial de Taveiro, Lote 8, 3045-508 Coimbra, Portugal (2018).

[33] M. J. Frisch, G. W. Trucks, H. B. Schlegel, G. E. Scuseria, M. A. Robb, J. R. Cheeseman, G. Scalmani, V. Barone, B. Mennucci, G. A. Petersson, H. Nakatsuji, M. Caricato, X. Li, H. P. Hratchian, A. F. Izmaylov, J. Bloino, G. Zheng, J. L. Sonnenberg, M. Hada, M. Ehara, K. Toyota, R. Fukuda, J. Hasegawa, M. Ishida, T. Nakajima, Y. Honda, O. Kitao, H. Nakai, T. Vreven, J. A. Montgomery, Jr., J. E. Peralta, F. Ogliaro, M. Bearpark, J. J. Heyd, E. Brothers, K. N. Kudin, V. N. Staroverov, R. Kobayashi, J. Normand, K. Raghavachari, A. Rendell, J. C. Burant, S. S. Iyengar, J. Tomasi, M. Cossi, N. Rega, J. M. Millam, M. Klene, J. E. Knox, J. B. Cross, V. Bakken, C. Adamo, J. Jaramillo, R. Gomperts, R. E. Stratmann, O. Yazyev, A. J. Austin, R. Cammi, C. Pomelli, J. W. Ochterski, R. L. Martin, K. Morokuma, V. G. Zakrzewski, G. A. Voth, P. Salvador, J. J. Dannenberg, S. Dapprich, A. D. Daniels, O. Farkas, J. B. Foresman, J. V. Ortiz, J. Cioslowski, D. J. Fox, Gaussian09, Revision A.01, Gaussian Inc. Wallingford CT (2009).

[34] A. E. Hansen, T. D. Bouman, Localized orbital/local origin method for calculation and analysis of NMR shieldings. applications to ^{13}C shielding tensors, The Journal of Chemical Physics 82 (11) (1985) 5035–5047. doi:10.1063/1.448625.

[35] S. N. Azizi, A. A. Rostami, A. Godarzian, ^{29}Si NMR chemical shift calculation for silicate species by gaussian software, Journal of the Physical Society of Japan 74 (5) (2005) 1609–1620. doi:10.1143/JPSJ.74.1609.

[36] C. Zhang, P. Patschinski, D. S. Stephenson, R. Panisch, J. H. Wender, M. C. Holthausen, H. Zipse, The calculation of ^{29}Si NMR chemical shifts of tetracoordinated silicon compounds in the gas phase and in solution, Phys. Chem. Chem. Phys. 16 (2014) 16642–16650. doi:10.1039/C4CP01736F.

[37] A. E. A. Fouda, N. A. Besley, Assessment of basis sets for density functional theory-based calculations of core-electron spectroscopies, Theoretical Chemistry Accounts 137 (1) (2017) 6. doi:10.1007/s00214-017-2181-0.

[38] G. Socrates, Infrared and Raman Characteristic Group Frequencies: Tables and Charts, Wiley, 2001.

[39] R. Al-Oweini, H. El-Rassy, Synthesis and characterization by FTIR spectroscopy of silica aerogels prepared using several $Si(OR)_4$ and $RSi(OR)_3$ precursors, Journal of Molecular Structure 919 (1) (2009) 140 – 145. doi:10.1016/j.molstruc.2008.08.025.

[40] T. B. Casserly, K. K. Gleason, Density functional theory calculation of ^{29}Si NMR chemical shifts of organosiloxanes, The Journal of Physical Chemistry B 109 (28) (2005) 13605–13610, pMID: 16852704. doi:10.1021/jp044385+.

[41] O. Filonenko, V. Kuts, M. Terebinska, V. Lobanov, Quantum-chemical calculation of ^{29}Si NMR spectrum of silicon dioxide fullerene-like molecules, Himia, Fizika ta Tehnologia Poverhni 6 (2) (2015) 263–268. doi:10.15407/hftp06.02.263.

[42] J. Šefčik, A. McCormick, Kinetic and thermodynamic issues in the early stages of sol-gel processes using silicon alkoxides, Catalysis Today 35 (3) (1997) 205 – 223, sol-gel Preparation of Catalytic Materials. doi:10.1016/S0920-5861(96)00158-7.

[43] B. N. Nguyen, M. A. B. Meador, M. E. Tousley, B. Shonkwiler, L. McCorkle, D. A. Scheiman, A. Palczer, Tailoring elastic properties of silica aerogels cross-linked with polystyrene, ACS Applied Materials & Interfaces 1 (3) (2009) 621–630, pMID: 20355984. doi:10.1021/am8001617.

Density functional theory based study of organically-modified silica aerogels

Supporting Information

*Pedro Maximiano**, Luísa Durães, Pedro N. Simões**

CIEPQPF, Department of Chemical Engineering, University of Coimbra, Rua Sílvio Lima, 3030-790 Coimbra, Portugal

*Corresponding author. Tel.: +351 239798732; E-mail address: pnsim@eq.uc.pt

**Corresponding author. Tel.: +351 239798702; E-mail address: pmsantos@eq.uc.pt

Silica clusters (oligomers) computationally studied in this work

Table A.1 – Set of silica clusters studied by DFT calculations for the aerogel of composition 50% TMOS/50% VTMS. The Q_m^n notation is used, where n denotes the number of Si atoms that are linked to other Si atoms by m -O- bridges. Each corner of the diagrams represents an Si atom and each edge a Si-O-Si link.

Type of structure	Configuration[a]		Symmetry point group	Code
Cage Q_8^3 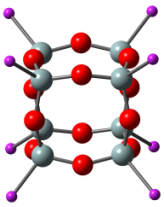	a	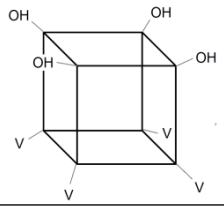	C2	TMVT_Q38_a_C2
			C1	TMVT_Q38_a_C1
	b	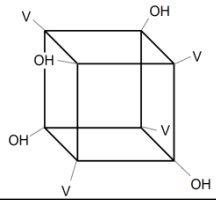	C2	TMVT_Q38_b_C2
			C1	TMVT_Q38_b_C1
	c	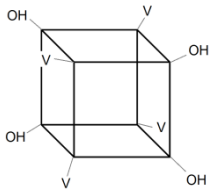	C2	TMVT_Q38_c_C2
			C1	TMVT_Q38_c_C1
	d	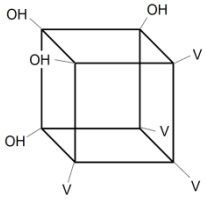	C1	TMVT_Q38_d_C1
	e	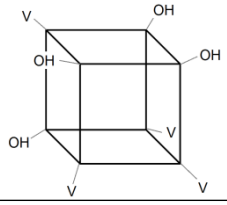	C1	TMVT_Q38_e_C1
	f	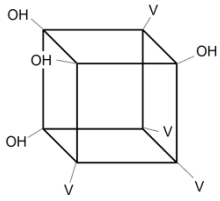	C1	TMVT_Q38_f_C1
Cyclic Q_3^2 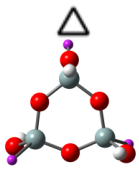		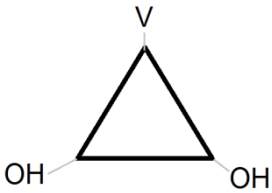	C1	TMVT_Q23_C1

[a] V = vynil  , OH = hydroxyl 

Table A.1 (continuation)

Type of structure	Configuration[a]		Symmetry point group	Code
Cyclic Q_4^2 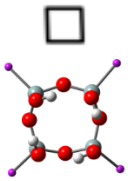	a	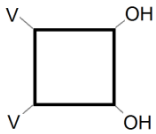	C1	TMVT_Q24_a_C1
	b	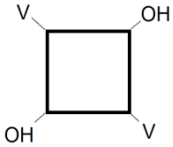	C2 C1	TMVT_Q24_b_C2 TMVT_Q24_b_C1
Cyclic $Q_2^2Q_1^3Q_1^1$ 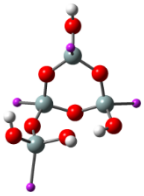	a	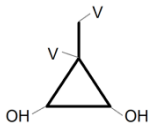	C1	TMVT_Q22Q31Q11_a_C1
	b	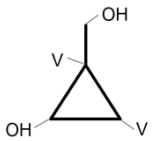	C1	TMVT_Q22Q31Q11_b_C1
	c	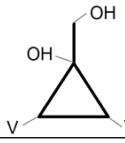	C1	TMVT_Q22Q31Q11_c_C1
	d	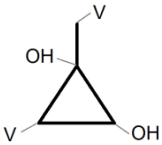	C1	TMVT_Q22Q31Q11_d_C1
Cyclic $Q_2^3Q_2^2$ 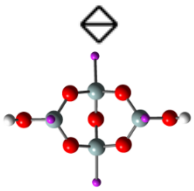	a	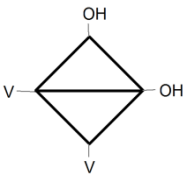	C1	TMVT_Q32Q22_a_C1
	b	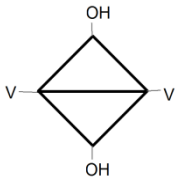	C2 C1	TMVT_Q32Q22_b_C2 TMVT_Q32Q22_b_C1
	c	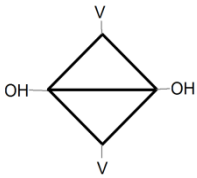	C2 C1	TMVT_Q32Q22_c_C2 TMVT_Q32Q22_c_C1
Linear Q_2^1 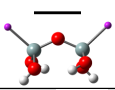		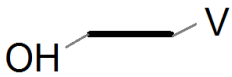	Cs C1	TMVT_Q12_Cs TMVT_Q12_C1

[a] V = vynil  , OH = hydroxyl 

Table A.1 (continuation)

Type of structure		Configuration[a]	Symmetry point group	Code
Linear $Q_2^2Q_2^1$  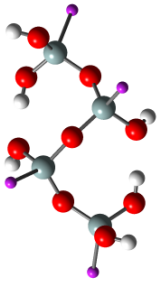	a	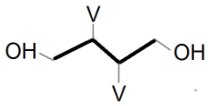	C1	TMVT_Q22Q12_a_C1
	b	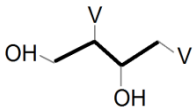	C1	TMVT_Q22Q12_b_C1
	c	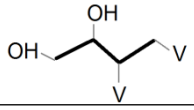	C1	TMVT_Q22Q12_c_C1
	d	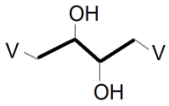	C2 C1	TMVT_Q22Q12_d_C2 TMVT_Q22Q12_d_C1
Linear $Q_3^1Q_1^3Q_1^2$ 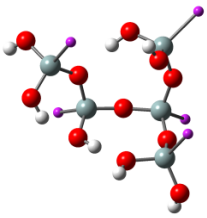	a	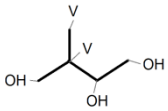	C1	TMVT_Q13Q31Q21_a_C1
	b	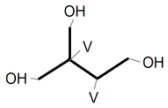	C1	TMVT_Q13Q31Q21_b_C1
	c	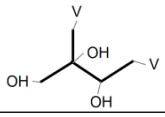	C1	TMVT_Q13Q31Q21_c_C1
	d	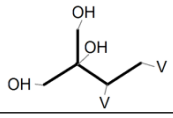	C1	TMVT_Q13Q31Q21_d_C1
	e	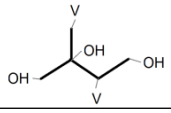	C1	TMVT_Q13Q31Q21_e_C1
	f	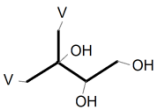	C1	TMVT_Q13Q31Q21_f_C1
Linear $Q_2^3Q_4^1$ 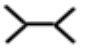 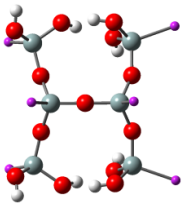	a	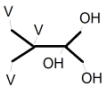	C1	TMVT_Q32Q14_a_C1
	b	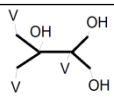	C1	TMVT_Q32Q14_b_C1
	c	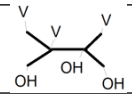	C1	TMVT_Q32Q14_c_C1
	d	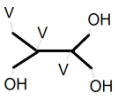	C1	TMVT_Q32Q14_d_C1
	e	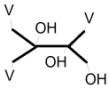	C1	TMVT_Q32Q14_e_C1

[a] V = vynil  , OH = hydroxyl 

Table A.1 (continuation)

Type of structure	Configuration[a]		Symmetry point group	Code
Linear $Q_1^4Q_1^3Q_5^1$ 	a	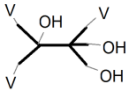	C1	TMVT_Q41Q31Q15_a_C1
	b	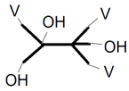	C1	TMVT_Q41Q31Q15_b_C1
	c	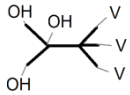	C1	TMVT_Q41Q31Q15_c_C1
	d	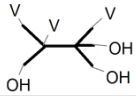	C1	TMVT_Q41Q31Q15_d_C1
	e	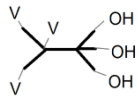	C1	TMVT_Q41Q31Q15_e_C1
	f	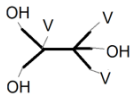	C1	TMVT_Q41Q31Q15_f_C1
Linear $Q_2^3Q_2^2Q_4^1$ 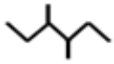 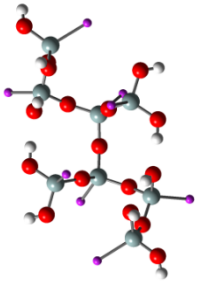	a	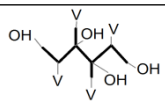	C1	TMVT_Q32Q22Q14_a_C1
	b	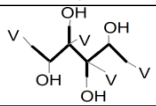	C1	TMVT_Q32Q22Q14_b_C1
	c	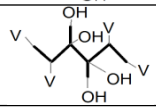	C1	TMVT_Q32Q22Q14_c_C1
	d	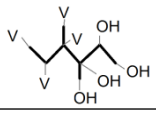	C1	TMVT_Q32Q22Q14_d_C1
	e	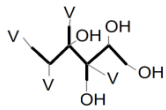	C1	TMVT_Q32Q22Q14_e_C1
	f	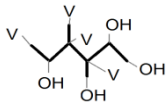	C1	TMVT_Q32Q22Q14_f_C1

[a] V = vynil  , OH = hydroxyl 

Table A.2 – Set of silica clusters studied by DFT calculations for the aerogel of composition 50% TMOS/50% APTMS. The Q_m^n notation is used, where n denotes the number of Si atoms that are linked to other Si atoms by m -O- bridges. Each corner of the diagrams represents an Si atom and each edge a Si-O-Si link.

Type of structure	Configuration[a]		Symmetry point group	Code
Cage Q_8^3 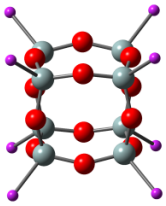	a	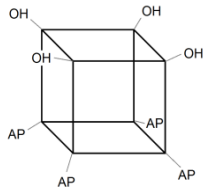	S4	TMAP_Q38_a_S4
			C1	TMAP_Q38_a_C1
	b	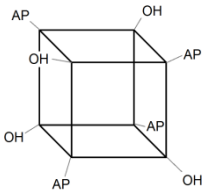	C2	TMAP_Q38_b_C2
			C1	TMAP_Q38_b_C1
	c	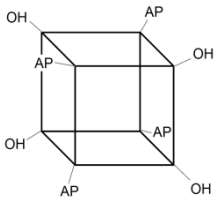	C2	TMAP_Q38_c_C2
			C1	TMAP_Q38_c_C1
	d	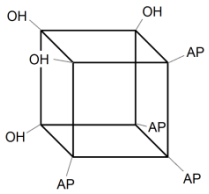	C1	TMAP_Q38_d_C1
	e	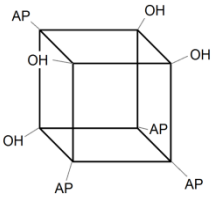	C1	TMAP_Q38_e_C1
	f	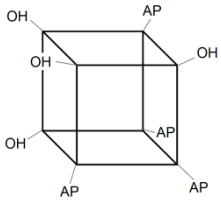	C1	TMAP_Q38_f_C1
Cyclic Q_3^2 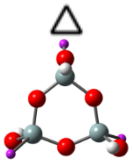		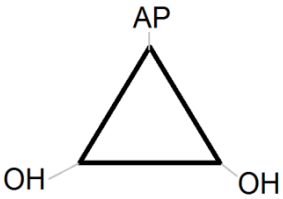	C1	TMAP_Q23_C1

[a] AP = aminopropyl ($-CH_2CH_2CH_2-NH_2$) ,  OH = hydroxyl 

Table A.2 (continuation)

Type of structure	Configuration[a]		Symmetry point group	Code
Cyclic Q_4^2 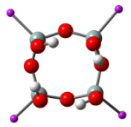	a	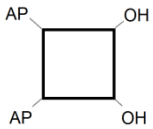	C1	TMAP_Q24_a_C1
	b	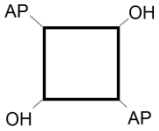	C2	TMAP_Q24_b_C2
			C1	TMAP_Q24_b_C1
Cyclic $Q_2^2Q_1^3Q_1^1$  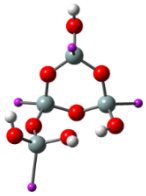	a	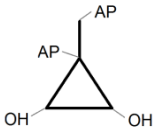	C1	TMAP_Q22Q31Q11_a_C1
	b	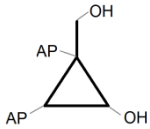	C1	TMAP_Q22Q31Q11_b_C1
	c	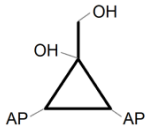	C1	TMAP_Q22Q31Q11_c_C1
	d	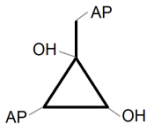	C1	TMAP_Q22Q31Q11_d_C1
Cyclic $Q_2^3Q_2^2$  	a	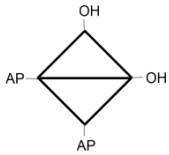	C1	TMAP_Q32Q22_a_C1
	b	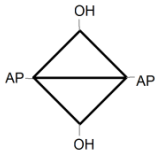	C2	TMAP_Q32Q22_b_C2
			C1	TMAP_Q32Q22_b_C1
	c	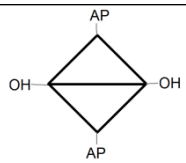	C2	TMAP_Q32Q22_c_C2
			C1	TMAP_Q32Q22_c_C1
Linear Q_2^1 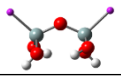	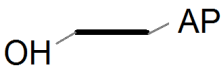		Cs	TMAP_Q12_Cs
			C1	TMAP_Q12_C1

[a] AP = aminopropyl ($-CH_2CH_2CH_2-NH_2$) ,  OH = hydroxyl 

Table A.2 (continuation)

Type of structure	Configuration[a]		Symmetry point group	Code
Linear $Q_2^2Q_2^1$  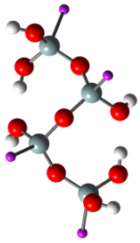	a	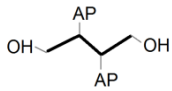	C2 C1	TMAP_Q22Q12_a_C2 TMAP_Q22Q12_a_C1
	b	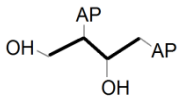	C1	TMAP_Q22Q12_b_C1
	c	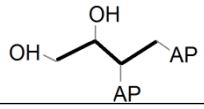	C1	TMAP_Q22Q12_c_C1
	d	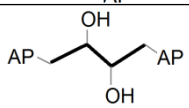	C2 C1	TMAP_Q22Q12_d_C2 TMAP_Q22Q12_d_C1
Linear $Q_3^1Q_1^3Q_1^2$ 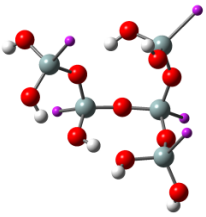	a	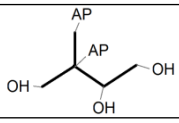	C1	TMAP_Q13Q31Q21_a_C1
	b	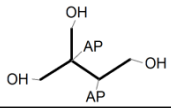	C1	TMAP_Q13Q31Q21_b_C1
	c	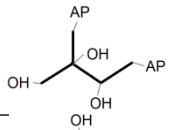	C1	TMAP_Q13Q31Q21_c_C1
	d	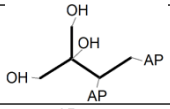	C1	TMAP_Q13Q31Q21_d_C1
	e	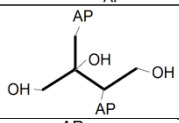	C1	TMAP_Q13Q31Q21_e_C1
	f	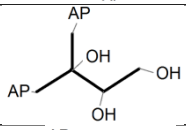	C1	TMAP_Q13Q31Q21_f_C1
Linear $Q_2^3Q_4^1$  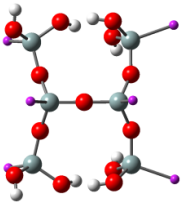	a	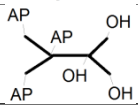	C1	TMAP_Q32Q14_a_C1
	b	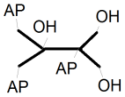	C1	TMAP_Q32Q14_b_C1
	c	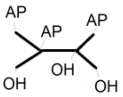	C1	TMAP_Q32Q14_c_C1
	d	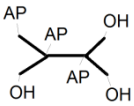	C1	TMAP_Q32Q14_d_C1
	e	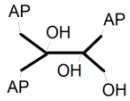	C1	TMAP_Q32Q14_e_C1

[a] AP = aminopropyl ($-CH_2CH_2CH_2-NH_2$) ,  OH = hydroxyl 

Table A.2 (continuation)

Type of structure	Configuration[a]		Symmetry point group	Code
Linear $Q_1^4Q_1^3Q_5^1$ 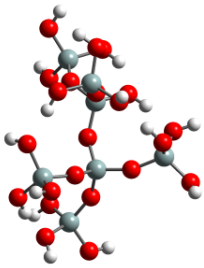	a	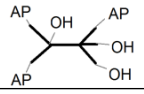	C1	TMAP_Q41Q31Q15_a_C1
	b	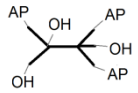	C1	TMAP_Q41Q31Q15_b_C1
	c	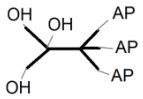	C1	TMAP_Q41Q31Q15_c_C1
	d	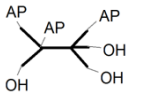	C1	TMAP_Q41Q31Q15_d_C1
	e	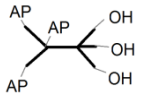	C1	TMAP_Q41Q31Q15_e_C1
	f	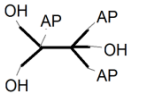	C1	TMAP_Q41Q31Q15_f_C1
Linear $Q_2^3Q_2^2Q_4^1$ 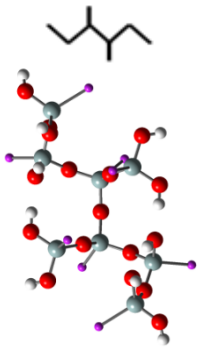	a	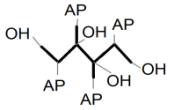	C1	TMAP_Q32Q22Q14_a_C1
	b	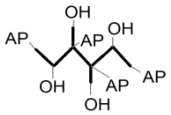	C1	TMAP_Q32Q22Q14_b_C1
	c	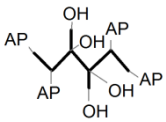	C1	TMAP_Q32Q22Q14_c_C1
	d	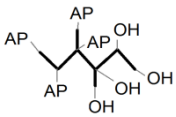	C1	TMAP_Q32Q22Q14_d_C1
	e	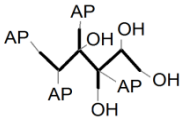	C1	TMAP_Q32Q22Q14_e_C1
	f	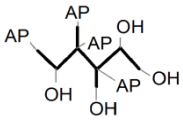	C1	TMAP_Q32Q22Q14_f_C1

[a] AP = aminopropyl ($-CH_2CH_2CH_2-NH_2$) ,  OH = hydroxyl 

Table A.3 – Set of silica clusters studied by DFT calculations for the aerogel of composition 50% TMOS/50% GLYMO. The Q_m^n notation is used, where n denotes the number of Si atoms that are linked to other Si atoms by m -O- bridges. Each corner of the diagrams represents an Si atom and each edge a Si-O-Si link.

Type of structure	Configuration[a]		Symmetry point group	Code
Cage Q_8^3  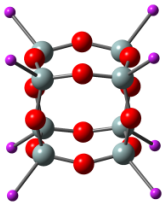	a	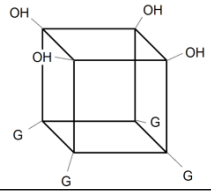	C2	TMG_Q38_a_C2
			C1	TMG_Q38_a_C1
	b	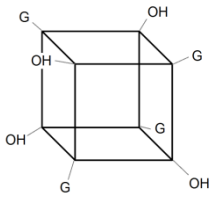	C2	TMG_Q38_b_C2
			C1	TMG_Q38_b_C1
	c	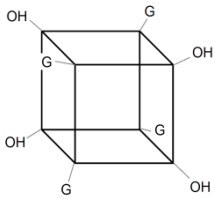	C2	TMG_Q38_c_C2
			C1	TMG_Q38_c_C1
	d	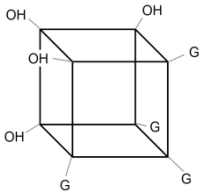	C1	TMG_Q38_d_C1
	e	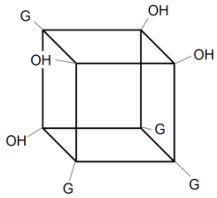	C1	TMG_Q38_e_C1
	f	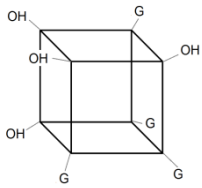	C1	TMG _Q38_f_C1
Cyclic Q_3^2 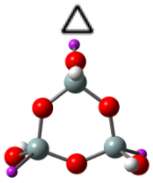	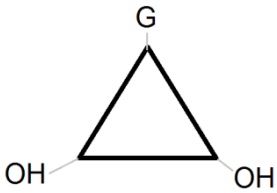		C1	TMG_Q23_C1

[a] G = glycidylpropoxy (-$CH_2CH_2CH_2$-O-CH_2-(-CH-CH_2-O-)) 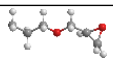 , OH = hydroxyl

Table A.3 (continuation)

Type of structure		Configuration[a]	Symmetry point group	Code
Cyclic Q_4^2 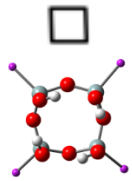	a	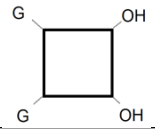	C1	TMG_Q24_a_C1
	b	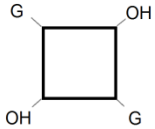	C2	TMG_Q24_b_C2
			C1	TMG_Q24_b_C1
Cyclic $Q_2^2Q_1^3Q_1^1$ 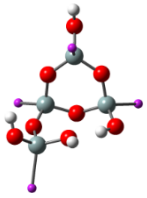	a	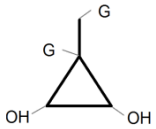	C1	TMG_Q22Q31Q11_a_C1
	b	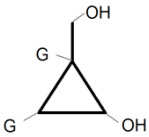	C1	TMG_Q22Q31Q11_b_C1
	c	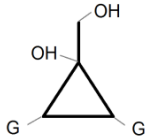	C1	TMG_Q22Q31Q11_c_C1
	d	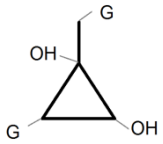	C1	TMG_Q22Q31Q11_d_C1
Cyclic $Q_2^3Q_2^2$ 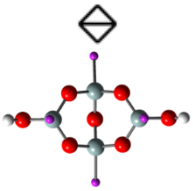	a	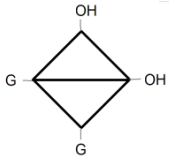	C1	TMG_Q32Q22_a_C1
	b	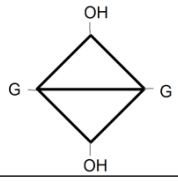	C2	TMG_Q32Q22_b_C2
			C1	TMG_Q32Q22_b_C1
	c	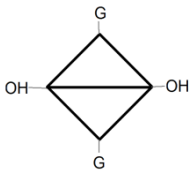	C2	TMG_Q32Q22_c_C2
			C1	TMG_Q32Q22_c_C1
Linear Q_2^1 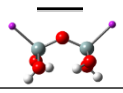			C1	TMG_Q12_C1

[a] G = glycidylpropoxy (-$CH_2CH_2CH_2$-O-CH_2-(-CH-CH_2-O-)) 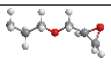 , OH = hydroxyl 

Table A.3 (continuation)

Type of structure	Configuration[a]		Symmetry point group	Code
Linear $Q_2^2Q_2^1$ 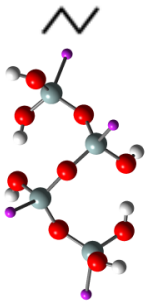	a	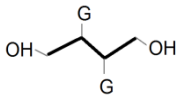	C2	TMG_Q22Q12_a_C2
			C1	TMG_Q22Q12_a_C1
	b	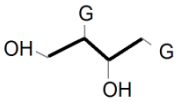	C1	TMG_Q22Q12_b_C1
	c	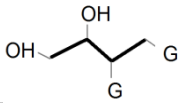	C1	TMG_Q22Q12_c_C1
	d	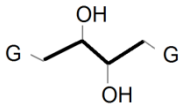	C2	TMG_Q22Q12_d_C2
			C1	TMG_Q22Q12_d_C1
Linear $Q_3^1Q_1^3Q_1^2$ 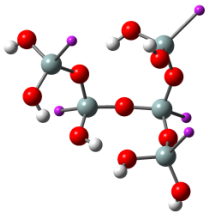	a	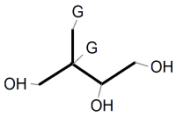	C1	TMG_Q13Q31Q21_a_C1
	b	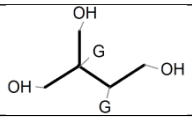	C1	TMG_Q13Q31Q21_b_C1
	c	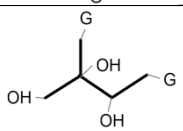	C1	TMG_Q13Q31Q21_c_C1
	d	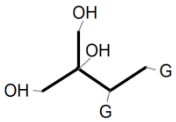	C1	TMG_Q13Q31Q21_d_C1
	e	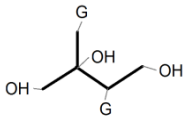	C1	TMG_Q13Q31Q21_e_C1
	f	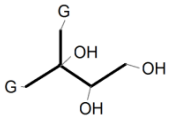	C1	TMG_Q13Q31Q21_f_C1
Linear $Q_2^3Q_4^1$ 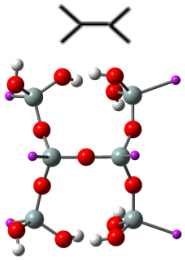	a	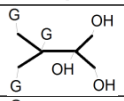	C1	TMG_Q32Q14_a_C1
	b	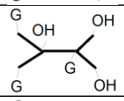	C1	TMG_Q32Q14_b_C1
	c	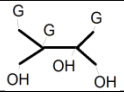	C1	TMG_Q32Q14_c_C1
	d	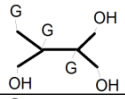	C1	TMG_Q32Q14_d_C1
	e	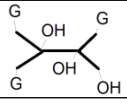	C1	TMG_Q32Q14_e_C1

[a] G = glycidylpropoxy (-$CH_2CH_2CH_2$-O-CH_2-(-CH-CH_2-O-)) 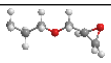 , OH = hydroxyl 

Table A.3 (continuation)

Type of structure		Configuration[a]	Symmetry point group	Code
Linear $Q_1^4Q_1^3Q_5^1$ 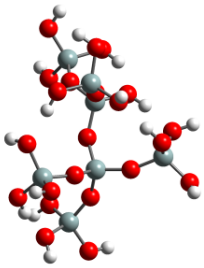	a	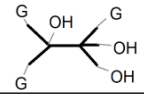	C1	TMG_Q41Q31Q15_a_C1
	b	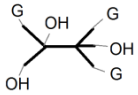	C1	TMG_Q41Q31Q15_b_C1
	c	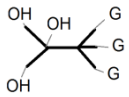	C1	TMG_Q41Q31Q15_c_C1
	d	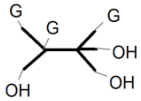	C1	TMG_Q41Q31Q15_d_C1
	e	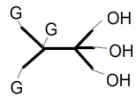	C1	TMG_Q41Q31Q15_e_C1
	f	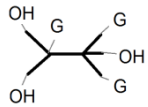	C1	TMG_Q41Q31Q15_f_C1
Linear $Q_2^3Q_2^2Q_4^1$ 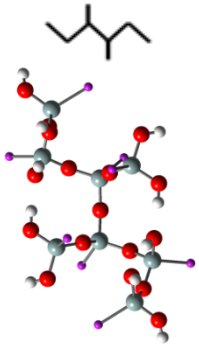	a	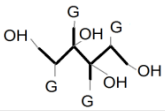	C1	TMG_Q32Q22Q14_a_C1
	b	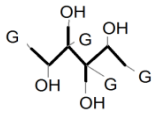	C1	TMG_Q32Q22Q14_b_C1
	c	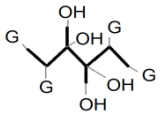	C1	TMG_Q32Q22Q14_c_C1
	d	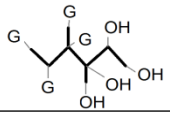	C1	TMG_Q32Q22Q14_d_C1
	e	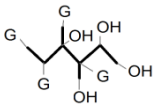	C1	TMG_Q32Q22Q14_e_C1
	f	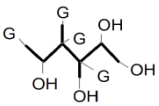	C1	TMG_Q32Q22Q14_f_C1

[a] G = glycidylpropoxy (-$CH_2CH_2CH_2$-O-CH_2-(-CH-CH_2-O-)) 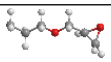 , OH = hydroxyl 

Results of the energy calculations

Table A.4 – Energies (E_{total}, kcal mol^{-1}), Gibbs free energy (G, kcal mol^{-1}), Gibbs free energy change ($\Delta_R G$, kcal mol^{-1}), normalized Gibbs free energy change ($\Delta_R G/s$, kcal mol^{-1}), rotational constants (MHz) and dipole moments (D) of silica clusters studied for the aerogel of composition 50% TMOS/50% VTMS (TMVT).

Species	B3LYP/6-311+G(d,p)				$\Delta_R G$ [b]	$\Delta_R G/s$ [c]	Rotational constants			Dipole moment
	E_{total} [a]	ΔE_{total}	G	ΔG			A	B	C	
TMVT_Q38_a_C2 [d]	-2406998.53	1.63	-2407042.63	1.96	-48.31	-6.04	108.72	108.26	100.58	1.73
TMVT_Q38_a_C1	-2406998.53	1.63	-2407042.63	1.96	-48.31	-6.04	108.73	108.25	100.58	1.73
TMVT_Q38_b_C2	-2407000.11	0.05	-2407042.42	2.17	-48.1	-6.01	108.92	103.78	103.78	0.00
TMVT_Q38_b_C1	-2406999.54	0.62	-2407042.63	1.96	-48.31	-6.04	109.19	108.62	99.31	1.47
TMVT_Q38_c_C2	-2406999.36	0.80	-2407041.83	2.76	-47.51	-5.94	119.74	103.69	95.77	2.61
TMVT_Q38_c_C1	-2407000.16	0.00	-2407043.28	1.31	-48.96	-6.12	112.55	108.99	96.13	0.01
TMVT_Q38_d_C1	-2406999.86	0.30	-2407043.00	1.59	-48.68	-6.09	111.15	103.20	103.03	1.50
TMVT_Q38_e_C1	-2406999.81	0.35	-2407043.36	1.23	-49.04	-6.13	115.91	103.92	98.28	1.83
TMVT_Q38_f_C1	**-2406999.77**	**0.39**	**-2407044.59**	**0.00**	**-50.27**	**-6.28**	**111.95**	**106.11**	**99.66**	**1.80**
TMVT_Q23_C1	**-1034056.13**	**0.00**	**-973932.17**	**0.00**	**-5.49**	**-1.83**	**651.54**	**502.06**	**369.54**	**0.58**
TMVT_Q24_a_C1	**-1299423.12**	**0.00**	**-1299457.16**	**0.00**	**-12.24**	**-3.06**	**326.71**	**300.21**	**185.42**	**1.30**
TMVT_Q24_b_C2	-1299421.21	1.91	-1299453.74	3.42	-8.82	-2.21	412.00	266.25	191.02	1.06
TMVT_Q24_b_C1	-1299421.22	1.90	-1299453.74	3.42	-8.82	-2.21	412.00	266.26	191.03	1.06
TMVT_Q22Q31Q11_a_C1	**-1299423.18**	**0.00**	**-1299455.51**	**0.00**	**-10.59**	**-2.65**	**379.09**	**235.66**	**221.67**	**0.61**
TMVT_Q22Q31Q11_b_C1	-1299422.72	0.46	-1299455.28	0.23	-10.36	-2.59	336.55	255.86	230.32	1.84
TMVT_Q22Q31Q11_c_C1	-1299419.62	3.56	-1299453.69	1.82	-8.77	-2.19	411.11	223.15	190.43	3.11
TMVT_Q22Q31Q11_d_C1	-1299422.01	1.17	-1299454.69	0.82	-9.77	-2.44	413.28	227.55	201.10	2.17
TMVT_Q32Q22_a_C1	**-1251444.69**	**0.00**	**-1251474.80**	**0.00**	**-3.76**	**-0.94**	**421.65**	**298.08**	**265.78**	**1.44**
TMVT_Q32Q22_b_C2	-1251443.08	1.61	-1251473.88	0.92	-2.84	-0.71	385.18	315.06	260.38	3.05
TMVT_Q32Q22_b_C1	-1251444.33	0.36	-1251474.60	0.20	-3.56	-0.89	353.14	325.39	301.74	4.98
TMVT_Q32Q22_c_C2 [d]	-1251442.66	2.03	-1251472.77	2.03	-1.73	-0.43	490.60	262.75	255.38	2.46
TMVT_Q32Q22_c_C1	-1251442.66	2.03	-1251472.77	2.03	-1.73	-0.43	490.59	262.76	255.38	2.46
TMVT_Q12_Cs [d]	**-697672.85**	**0.00**	**-697698.95**	**0.00**	**-2.61**	**-1.30**	**1829.59**	**562.33**	**558.20**	**1.84**
TMVT_Q12_C1	-697672.44	0.41	-697698.42	0.53	-2.08	-1.04	1751.90	565.46	538.46	2.14
TMVT_Q22Q12_a_C1	-1347388.83	3.39	-1347426.33	2.47	-7.53	-1.88	386.81	170.94	144.40	1.63
TMVT_Q22Q12_b_C1	**-1347392.22**	**0.00**	**-1347428.80**	**0.00**	**-10.00**	**-2.50**	**416.96**	**159.35**	**143.93**	**2.00**
TMVT_Q22Q12_c_C1	-1347390.87	1.35	-1347428.32	0.48	-9.52	-2.38	388.31	159.59	146.35	3.74
TMVT_Q22Q12_d_C2	-1347389.37	2.85	-1347426.22	2.58	-7.42	-1.85	489.34	137.63	133.58	0.52
TMVT_Q22Q12_d_C1	-1347390.71	1.51	-1347426.93	1.87	-8.13	-2.03	479.71	142.11	140.52	4.62
TMVT_Q13Q31Q21_a_C1	-1671596.02	2.03	-1671634.82	3.63	-11.8	-2.36	188.80	163.64	154.46	5.74
TMVT_Q13Q31Q21_b_C1	-1671595.80	2.25	-1671634.81	3.64	-11.79	-2.36	210.14	159.32	146.71	6.11
TMVT_Q13Q31Q21_c_C1	**-1671598.05**	**0.00**	**-1671638.45**	**0.00**	**-15.43**	**-3.09**	**204.79**	**146.68**	**138.53**	**3.02**
TMVT_Q13Q31Q21_d_C1	-1671595.85	2.20	-1671635.14	3.31	-12.12	-2.42	215.96	151.05	143.76	4.00
TMVT_Q13Q31Q21_e_C1	-1671597.01	1.04	-1671636.10	2.35	-13.08	-2.62	198.14	162.72	144.41	4.25
TMVT_Q13Q31Q21_f_C1	-1671596.78	1.27	-1671635.53	2.92	-12.51	-2.50	198.57	164.75	138.70	3.70

Table A.4 (continuation)

Species	B3LYP/6-311+G(d,p)				$\Delta_R G$ [b]	$\Delta_R G/s$ [c]	Rotational constants			Dipole moment
	E_{total} [a]	ΔE_{total}	G	ΔG		E_{total} [a]	A	B	C	
TMVT_Q32Q14_a_C1	-1997110.44	10.82	-1997156.67	1.30	-15.41	-2.57	153.86	103.43	92.84	4.10
TMVT_Q32Q14_b_C1	-1997109.93	5.91	-1997156.82	1.15	-15.56	-2.59	155.49	103.74	89.95	5.14
TMVT_Q32Q14_c_C1	-1997110.76	0.00	-1997157.16	0.81	-15.9	-2.65	146.56	107.82	91.34	5.40
TMVT_Q32Q14_d_C1	-1997110.88	1.59	-1997156.82	1.15	-15.56	-2.59	145.30	111.30	97.90	4.13
TMVT_Q32Q14_e_C1	**-1997110.82**	**7.60**	**-1997157.97**	**0.00**	**-16.71**	**-2.79**	**152.31**	**100.84**	**86.99**	**4.62**
TMVT_Q41Q31Q15_a_C1	-2321319.08	2.82	-2321367.37	2.60	-21.89	-3.13	98.45	94.82	69.98	4.17
TMVT_Q41Q31Q15_b_C1	-2321320.50	1.40	-2321368.77	1.20	-23.29	-3.33	106.80	89.78	69.46	3.63
TMVT_Q41Q31Q15_c_C1	**-2321321.90**	**0.00**	**-2321369.97**	**0.00**	**-24.49**	**-3.50**	**100.94**	**89.53**	**72.78**	**2.53**
TMVT_Q41Q31Q15_d_C1	-2321318.16	3.74	-2321367.53	2.44	-22.05	-3.15	98.94	93.33	70.89	4.61
TMVT_Q41Q31Q15_e_C1	-2321318.54	3.36	-2321367.61	2.36	-22.13	-3.16	100.76	93.04	71.99	4.14
TMVT_Q41Q31Q15_f_C1	-2321316.47	5.43	-2321366.53	3.44	-21.05	-3.01	100.17	92.29	69.77	3.34
TMVT_Q32Q22Q14_a_C1	-2646829.37	11.77	-2646883.73	11.72	-20.01	-2.50	82.02	71.09	60.26	2.22
TMVT_Q32Q22Q14_b_C1	-2646841.14	0.00	-2646894.90	0.55	-31.18	-3.90	75.11	72.97	65.46	1.75
TMVT_Q32Q22Q14_c_C1	-2646834.60	6.54	-2646890.94	4.51	-27.22	-3.40	99.39	49.12	45.17	1.24
TMVT_Q32Q22Q14_d_C1	-2646835.62	5.52	-2646890.00	5.45	-26.28	-3.29	77.20	71.02	65.10	2.83
TMVT_Q32Q22Q14_e_C1	**-2646841.04**	**0.10**	**-2646895.45**	**0.00**	**-31.73**	**-3.97**	**81.79**	**64.56**	**61.64**	**3.58**
TMVT_Q32Q22Q14_f_C1	-2646839.55	1.59	-2646892.68	2.77	-28.96	-3.62	77.94	70.07	65.93	3.11

[a] Total electronic energy, with zero-point energy (ZPE) correction estimated by vibrational analysis at 298 K.

[b] Gibbs free energy change in the condensation reaction: Hydrolyzed Precursors $\leftrightarrow$ Cluster + H_2O: $\Delta_R G = G(\text{cluster}) + n_{H2O} \times G(H_2O) - n_{VTMS} \times G(\text{VTMS}) - n_{TMOS} \times G(\text{TMOS})$ (at the B3LYP/6-311+G(d,p) level of theory: $G(H_2O)$ = -47973.88 kcal mol^{-1}, G(VTMS) = -373492.12 kcal mol^{-1}, G(TMOS) = -372178.10 kcal mol^{-1}.

[c] Gibbs free energy change in the condensation reaction normalized by the number of Si atoms in the cluster, s (number of precursor molecules used to form the cluster)

[d] These clusters yielded saddle points, which upon further processing of imaginary frequency coordinates and optimization, resulted in a structure with C1 symmetry.

Table A.5 – Energies (E_{total}, kcal mol^{-1}), Gibbs free energy (G, kcal mol^{-1}), Gibbs free energy change ($\Delta_R G$, kcal mol^{-1}), normalized Gibbs free energy change ($\Delta_R G/s$, kcal mol^{-1}), rotational constants (MHz) and dipole moments (D) of silica clusters studied for the aerogel of composition 50% TEOS/50% APTES (TMAP).

Species	B3LYP/6-311+G(d,p)				$\Delta_R G$ [b]	$\Delta_R G/s$ [c]	Rotational constants			Dipole moment
	E_{total} [a]	ΔE_{total}	G	ΔG			A	B	C	
TMAP_Q38_a_S4	-2647606.97	2.77	-2647657.24	8.53	-43.04	-5.38	69.57	48.40	48.40	0.00
TMAP_Q38_a_C1	-2647608.15	1.59	-2647663.71	2.06	-49.51	-6.19	66.55	58.78	52.95	3.31
TMAP_Q38_b_C2	-2647609.05	0.69	-2647664.01	1.76	-49.81	-6.23	71.85	54.62	54.14	1.54
TMAP_Q38_b_C1	-2647609.73	0.01	-2647663.48	2.29	-49.28	-6.16	65.15	62.01	49.86	4.31
TMAP_Q38_c_C2 [d]	-2647609.74	0.00	-2647665.72	0.05	-51.52	-6.44	71.60	57.09	41.85	4.76
TMAP_Q38_c_C1	-2647608.49	1.25	-2647663.31	2.46	-49.11	-6.14	82.29	54.13	45.21	2.31
TMAP_Q38_d_C1	-2647608.85	0.89	-2647665.29	0.48	-51.09	-6.39	67.90	54.14	48.90	5.13
TMAP_Q38_e_C1	**-2647608.94**	**0.80**	**-2647665.77**	**0.00**	**-51.57**	**-6.45**	**66.53**	**54.92**	**47.78**	**1.95**
TMAP_Q38_f_C1	-2647608.72	1.02	-2647665.69	0.08	-51.49	-6.44	75.40	55.36	46.01	3.64
TMAP_Q23_C1	**-1034056.13**	**0.00**	**-1034087.80**	**0.00**	**-6.15**	**-2.05**	**591.68**	**255.88**	**221.61**	**1.59**
TMAP_Q24_a_C1	-1419727.34	0.00	-1419767.87	0.10	-13.01	-3.25	226.06	146.93	100.18	1.28
TMAP_Q24_b_C2	-1419726.26	1.08	-1419765.06	2.91	-10.2	-2.55	244.60	121.13	119.54	0.96
TMAP_Q24_b_C1	**-1419725.75**	**1.59**	**-1419767.97**	**0.00**	**-13.11**	**-3.28**	**258.23**	**121.39**	**102.53**	**3.42**
TMAP_Q22Q31Q11_a_C1	-1419727.29	0.00	-1419766.30	0.01	-11.44	-2.86	204.40	139.29	104.82	1.52
TMAP_Q22Q31Q11_b_C1	**-1419727.20**	**0.09**	**-1419766.31**	**0.00**	**-11.45**	**-2.86**	**183.18**	**154.85**	**119.16**	**1.43**
TMAP_Q22Q31Q11_c_C1	-1419724.18	3.11	-1419764.33	1.98	-9.47	-2.37	200.50	147.81	103.74	4.09
TMAP_Q22Q31Q11_d_C1	-1419725.95	1.34	-1419764.78	1.53	-9.92	-2.48	274.60	108.72	91.99	2.45
TMAP_Q32Q22_a_C1	-1371747.76	1.68	-1371784.37	1.72	-3.39	-0.85	217.89	183.47	124.78	3.16
TMAP_Q32Q22_b_C2	-1371747.41	2.03	-1371785.02	1.07	-4.04	-1.01	313.43	129.79	116.65	4.55
TMAP_Q32Q22_b_C1	**-1371749.44**	**0.00**	**-1371786.09**	**0.00**	**-5.11**	**-1.28**	**327.41**	**126.91**	**121.20**	**5.21**
TMAP_Q32Q22_c_C2 [d]	-1371747.82	1.62	-1371784.39	1.70	-3.41	-0.85	452.24	118.51	115.22	2.59
TMAP_Q32Q22_c_C1	-1371747.82	1.62	-1371784.40	1.69	-3.42	-0.85	452.24	118.51	115.22	2.59
TMAP_Q12_Cs [d]	-757824.09	0.33	-757852.98	0.69	-1.67	-0.83	1418.67	293.39	276.15	1.85
TMAP_Q12_C1	**-757824.42**	**0.00**	**-757853.67**	**0.00**	**-2.36**	**-1.18**	**1522.47**	**280.10**	**268.70**	**2.72**
TMAP_Q22Q12_a_C2	-1467696.82	0.04	-1467740.32	0.32	-11.58	-2.89	202.71	103.79	93.01	1.28
TMAP_Q22Q12_a_C1	**-1467696.86**	**0.00**	**-1467740.64**	**0.00**	**-11.9**	**-2.97**	**203.35**	**103.61**	**93.19**	**1.30**
TMAP_Q22Q12_b_C1	-1467696.09	0.77	-1467738.43	2.21	-9.69	-2.42	281.00	95.19	85.76	1.07
TMAP_Q22Q12_c_C1	-1467694.67	2.19	-1467738.41	2.23	-9.67	-2.42	203.69	101.01	79.07	4.10
TMAP_Q22Q12_d_C2	-1467693.95	2.91	-1467737.60	3.04	-8.86	-2.21	388.55	74.55	73.60	3.99
TMAP_Q22Q12_d_C1	-1467694.69	2.17	-1467737.64	3.00	-8.9	-2.22	272.61	80.29	72.60	5.41
TMAP_Q13Q31Q21_a_C1	-1791900.67	1.08	-1791946.10	1.44	-13.14	-2.63	159.61	98.71	86.74	5.70
TMAP_Q13Q31Q21_b_C1	-1791899.61	2.14	-1791944.85	2.69	-11.89	-2.38	142.16	116.34	88.62	6.93
TMAP_Q13Q31Q21_c_C1	-1791901.00	0.75	-1791946.34	1.20	-13.38	-2.68	135.94	96.35	81.26	2.73
TMAP_Q13Q31Q21_d_C1	-1791900.35	1.40	-1791945.95	1.59	-12.99	-2.60	127.58	112.27	82.11	3.89
TMAP_Q13Q31Q21_e_C1	**-1791901.75**	**0.00**	**-1791947.54**	**0.00**	**-14.58**	**-2.92**	**136.80**	**99.02**	**82.73**	**3.90**
TMAP_Q13Q31Q21_f_C1	-1791900.79	0.96	-1791946.06	1.48	-13.1	-2.62	128.02	98.83	73.28	5.21

Table A.5 (continuation)

Species	B3LYP/6-311+G(d,p)				$\Delta_R G$ [b]	$\Delta_R G/s$ [c]	Rotational constants			Dipole moment
	E_{total} [a]	ΔE_{total}	G	ΔG			A	B	C	
TMAP_Q32Q14_a_C1	-2177570.85	0.58	-2177623.91	2.52	-17.74	-2.96	99.06	66.54	56.05	3.47
TMAP_Q32Q14_b_C1	**-2177570.92**	**0.51**	**-2177626.43**	**0.00**	**-20.26**	**-3.38**	**93.64**	**62.45**	**46.62**	**5.69**
TMAP_Q32Q14_c_C1	-2177571.43	0.00	-2177624.12	2.31	-17.95	-2.99	84.43	68.26	55.29	7.76
TMAP_Q32Q14_d_C1	-2177567.63	3.80	-2177621.63	4.80	-15.46	-2.58	92.99	67.89	64.72	3.93
TMAP_Q32Q14_e_C1	-2177567.93	3.50	-2177621.11	5.32	-14.94	-2.49	76.61	62.61	49.34	2.51
TMAP_Q41Q31Q15_a_C1	-2501776.57	6.03	-2501833.95	5.62	-23.56	-3.37	71.09	56.47	40.55	3.26
TMAP_Q41Q31Q15_b_C1	-2501776.08	6.52	-2501834.14	5.43	-23.75	-3.39	73.70	49.63	36.28	3.71
TMAP_Q41Q31Q15_c_C1	-2501777.04	5.56	-2501834.72	4.85	-24.33	-3.48	57.42	55.34	42.24	3.67
TMAP_Q41Q31Q15_d_C1	-2501775.38	7.22	-2501833.16	6.41	-22.77	-3.25	72.65	58.38	46.00	4.20
TMAP_Q41Q31Q15_e_C1	-2501774.58	8.02	-2501833.91	5.66	-23.52	-3.36	64.40	58.85	46.71	6.67
TMAP_Q41Q31Q15_f_C1	**-2501782.60**	**0.00**	**-2501839.57**	**0.00**	**-29.18**	**-4.17**	**70.06**	**58.93**	**46.03**	**2.09**
TMAP_Q32Q22Q14_a_C1	-2887444.82	9.51	-2887509.32	8.72	-25.72	-3.21	48.51	44.05	29.62	3.98
TMAP_Q32Q22Q14_b_C1	**-2887454.33**	**0.00**	**-2887518.04**	**0.00**	**-34.44**	**-4.31**	**56.72**	**43.17**	**34.95**	**3.20**
TMAP_Q32Q22Q14_c_C1	-2887443.18	11.15	-2887511.22	6.82	-27.62	-3.45	52.56	38.73	33.45	1.12
TMAP_Q32Q22Q14_d_C1	-2887443.52	10.81	-2887509.07	8.97	-25.47	-3.18	48.18	45.45	40.03	5.60
TMAP_Q32Q22Q14_e_C1	-2887449.58	4.75	-2887515.73	2.31	-32.13	-4.02	49.36	40.03	35.72	5.39
TMAP_Q32Q22Q14_f_C1	-2887448.42	5.91	-2887514.57	3.47	-30.97	-3.87	48.61	42.60	37.08	3.31

[a] Total electronic energy, with zero-point energy (ZPE) correction estimated by vibrational analysis at 298 K.

[b] Gibbs free energy change in the condensation reaction: Hydrolyzed Precursors $\leftrightarrow$ Cluster + H_2O: $\Delta_R G = G(\text{cluster}) + n_{H2O} \times G(H_2O) - n_{APTES} \times G(\text{APTES}) - n_{TMOS} \times G(\text{TEOS})$ (at the B3LYP/6-311+G(d,p) level of theory: $G(H_2O)$ = -47973.88 kcal mol^{-1}, G(APTES) = -433647.09 kcal mol^{-1}, G(TEOS) = -372178.10 kcal mol^{-1}.

[c] Gibbs free energy change in the condensation reaction normalized by the number of Si atoms in the cluster, s (number of precursor molecules used to form the cluster)

[d] These clusters yielded saddle points, which upon further processing of imaginary frequency coordinates and optimization, resulted in a structure with C1 symmetry.

Table A.6 – Energies (E_{total}, kcal mol^{-1}), Gibbs free energy (G, kcal mol^{-1}), Gibbs free energy change ($\Delta_R G$, kcal mol^{-1}), normalized Gibbs free energy change ($\Delta_R G/s$, kcal mol^{-1}), rotational constants (MHz) and dipole moments (D) of silica clusters studied for the aerogel of composition 50% TEOS/50% GLYMO (TMG).

Species	B3LYP/6-311+G(d,p)				$\Delta_R G$ [b]	$\Delta_R G/s$ [c]	Rotational constants			Dipole moment
	E_{total} [a]	ΔE_{total}	G	ΔG			A	B	C	
TMG_Q38_a_C2	-3179158.64	1.40	-3179232.15	2.39	-48.59	-6.07	33.17	22.24	22.04	5.48
TMG_Q38_a_C1	-3179155.71	4.33	-3179228.94	5.60	-45.38	-5.67	38.11	25.34	22.89	5.91
TMG_Q38_b_C2	-3179159.27	0.77	-3179233.20	1.34	-49.64	-6.21	22.74	21.75	15.98	1.17
TMG_Q38_b_C1	-3179160.04	0.00	-3179234.35	0.19	-50.79	-6.35	23.96	20.53	19.31	1.03
TMG_Q38_c_C2	-3179156.00	4.04	-3179230.78	3.76	-47.22	-5.90	33.01	20.12	13.95	3.57
TMG_Q38_c_C1	**-3179159.91**	**0.13**	**-3179234.54**	**0.00**	**-50.98**	**-6.37**	**35.46**	**21.40**	**15.02**	**1.77**
TMG_Q38_d_C1	-3179159.15	0.89	-3179233.47	1.07	-49.91	-6.24	27.03	20.90	20.31	3.44
TMG_Q38_e_C1	-3179156.40	3.64	-3179232.02	2.52	-48.46	-6.06	30.78	22.31	15.34	2.51
TMG_Q38_f_C1	-3179159.39	0.65	-3179234.13	0.41	-50.57	-6.32	30.77	20.90	16.40	2.51
TMG_Q23_C1	**-1166943.72**	**0.00**	**-1166980.62**	**0.00**	**-6.63**	**-2.21**	**559.50**	**94.18**	**89.26**	**3.49**
TMG_Q24_a_C1	-1685502.68	0.90	-1685551.64	0.87	-12.1	-3.02	109.63	58.35	39.98	2.79
TMG_Q24_b_C2	-1685501.09	2.49	-1685549.05	3.46	-9.51	-2.38	98.24	53.20	40.28	3.64
TMG_Q24_b_C1	**-1685503.58**	**0.00**	**-1685552.51**	**0.00**	**-12.97**	**-3.24**	**133.68**	**60.57**	**50.39**	**4.93**
TMG_Q22Q31Q11_a_C1	-1685500.70	1.54	-1685548.68	1.66	-9.14	-2.28	102.34	52.02	38.38	1.34
TMG_Q22Q31Q11_b_C1	**-1685502.24**	**0.00**	**-1685550.34**	**0.00**	-10.8	-2.70	78.86	68.05	42.88	2.80
TMG_Q22Q31Q11_c_C1	-1685497.55	4.69	-1685547.29	3.05	-7.75	-1.94	103.98	64.10	44.66	4.27
TMG_Q22Q31Q11_d_C1	-1685500.32	1.92	-1685548.80	1.54	-9.26	-2.32	98.70	48.88	35.57	3.23
TMG_Q32Q22_a_C1	-1637521.70	3.62	-1637569.23	2.49	-3.57	-0.89	84.46	73.76	43.30	1.25
TMG_Q32Q22_b_C2 [d]	**-1637525.32**	**0.00**	**-1637571.72**	**0.00**	**-6.06**	**-1.51**	**293.75**	**36.19**	**35.97**	**2.64**
TMG_Q32Q22_b_C1	-1637523.85	1.47	-1637570.06	1.66	-4.4	-1.10	187.15	43.60	40.63	3.02
TMG_Q32Q22_c_C2 [d]	-1637522.45	2.87	-1637568.10	3.62	-2.44	-0.61	227.94	40.09	36.72	2.88
TMG_Q32Q22_c_C1	-1637523.00	2.32	-1637569.03	2.69	-3.37	-0.84	385.24	38.07	37.83	0.70
TMG_Q12_C1	**-890711.92**	**0.00**	**-890745.62**	**0.00**	**-1.97**	**-0.98**	**1548.96**	**102.29**	**101.39**	**1.82**
TMG_Q22Q12_a_C2	**-1733471.74**	**0.97**	**-1733525.62**	**0.00**	**-12.2**	**-3.05**	**130.86**	**35.68**	**35.40**	**2.27**
TMG_Q22Q12_a_C1	-1733471.61	1.10	-1733524.69	0.93	-11.27	-2.82	130.50	35.80	35.27	2.22
TMG_Q22Q12_b_C1	-1733471.71	1.00	-1733523.66	1.96	-10.24	-2.56	137.04	32.58	28.60	2.06
TMG_Q22Q12_c_C1	-1733472.71	0.00	-1733523.71	1.91	-10.29	-2.57	93.52	45.66	33.06	2.19
TMG_Q22Q12_d_C2 [d]	-1733471.81	0.90	-1733523.74	1.88	-10.32	-2.58	113.59	34.81	28.78	6.20
TMG_Q22Q12_d_C1	-1733471.97	0.74	-1733523.35	2.27	-9.93	-2.48	146.75	30.82	27.55	2.01
TMG_Q13Q31Q21_a_C1	-2057675.45	1.48	-2057729.48	2.28	-11.84	-2.37	85.94	47.62	36.54	4.49
TMG_Q13Q31Q21_b_C1	-2057675.94	0.99	-2057730.87	0.89	-13.23	-2.65	82.41	53.11	40.20	2.21
TMG_Q13Q31Q21_c_C1	-2057675.70	1.23	-2057730.48	1.28	-12.84	-2.57	78.43	38.85	30.53	3.81
TMG_Q13Q31Q21_d_C1	-2057673.27	3.66	-2057727.31	4.45	-9.67	-1.93	102.07	38.56	32.59	1.04
TMG_Q13Q31Q21_e_C1	**-2057676.93**	**0.00**	**-2057731.76**	**0.00**	**-14.12**	**-2.82**	**112.57**	**34.51**	**29.95**	**2.80**
TMG_Q13Q31Q21_f_C1	-2057675.24	1.69	-2057729.27	2.49	-11.63	-2.33	83.61	36.46	28.63	4.00

Table A.6 (continuation)

Species	B3LYP/6-311+G(d,p)				$\Delta_R G$ [b]	$\Delta_R G/s$ [c]	Rotational constants			Dipole moment
	E_{total} [a]	ΔE_{total}	G	ΔG			A	B	C	
TMG_Q32Q14_a_C1	-2576226.04	10.82	-2576295.18	9.50	-11.99	-2.00	51.48	26.94	22.46	7.73
TMG_Q32Q14_b_C1	-2576230.95	5.91	-2576299.75	4.93	-16.56	-2.76	58.65	25.98	20.42	2.98
TMG_Q32Q14_c_C1	**-2576236.86**	**0.00**	**-2576304.68**	**0.00**	**-21.49**	**-3.58**	39.35	23.65	19.99	0.99
TMG_Q32Q14_d_C1	-2576235.27	1.59	-2576302.18	2.50	-18.99	-3.17	44.99	30.86	25.99	6.58
TMG_Q32Q14_e_C1	-2576229.26	7.60	-2576297.03	7.65	-13.84	-2.31	52.68	20.76	16.93	5.20
TMG_Q41Q31Q15_a_C1	-2900439.21	0.00	-2900511.22	1.00	-23.81	-3.40	33.44	22.46	14.86	3.89
TMG_Q41Q31Q15_b_C1	-2900438.25	0.96	-2900510.28	1.94	-22.87	-3.27	46.57	20.76	15.96	3.12
TMG_Q41Q31Q15_c_C1	-2900438.95	0.26	-2900510.64	1.58	-23.23	-3.32	35.99	24.98	20.21	2.44
TMG_Q41Q31Q15_d_C1	**-2900438.53**	**0.68**	**-2900512.22**	**0.00**	**-24.81**	**-3.54**	31.32	30.42	20.12	5.53
TMG_Q41Q31Q15_e_C1	-2900436.21	3.00	-2900509.56	2.66	-22.15	-3.16	32.18	23.34	20.05	5.77
TMG_Q41Q31Q15_f_C1	-2900438.32	0.89	-2900511.76	0.46	-24.35	-3.48	32.57	26.82	20.90	5.67
TMG_Q32Q22Q14_a_C1	-3418998.51	3.25	-3419082.66	2.44	-29.7	-3.71	20.24	17.49	12.48	2.65
TMG_Q32Q22Q14_b_C1	-3419001.76	0.00	-3419083.23	1.87	-30.27	-3.78	25.63	20.01	14.11	3.44
TMG_Q32Q22Q14_c_C1	-3418991.49	10.27	-3419077.79	7.31	-24.83	-3.10	41.30	10.98	10.65	2.66
TMG_Q32Q22Q14_d_C1	-3418999.57	2.19	-3419083.36	1.74	-30.4	-3.80	21.59	19.12	16.27	2.50
TMG_Q32Q22Q14_e_C1	**-3419001.45**	**0.31**	**-3419085.10**	**0.00**	**-32.14**	**-4.02**	28.05	19.33	15.25	3.07
TMG_Q32Q22Q14_f_C1	-3418998.13	3.63	-3419081.11	3.99	-28.15	-3.52	32.24	17.82	14.16	0.58

[a] Total electronic energy, with zero-point energy (ZPE) correction estimated by vibrational analysis at 298 K.

[b] Gibbs free energy change in the condensation reaction: Hydrolyzed Precursors $\leftrightarrow$ Cluster + H_2O: $\Delta_R G = G(\text{cluster}) + n_{H2O} \times G(H_2O) - n_{GLYMO} \times G(\text{GLYMO}) - n_{TMOS} \times G(\text{TEOS})$ (at the B3LYP/6-311+G(d,p) level of theory: $G(H_2O)$ = -47973.88 kcal mol^{-1}, G(GLYMO) = -566539.43 kcal mol^{-1}, G(TEOS) = -372178.10 kcal mol^{-1}.

[c] Gibbs free energy change in the condensation reaction normalized by the number of Si atoms in the cluster, s (number of precursor molecules used to form the cluster)

[d] These clusters yielded saddle points, which upon further processing of imaginary frequency coordinates and optimization, resulted in a structure with C1 symmetry.

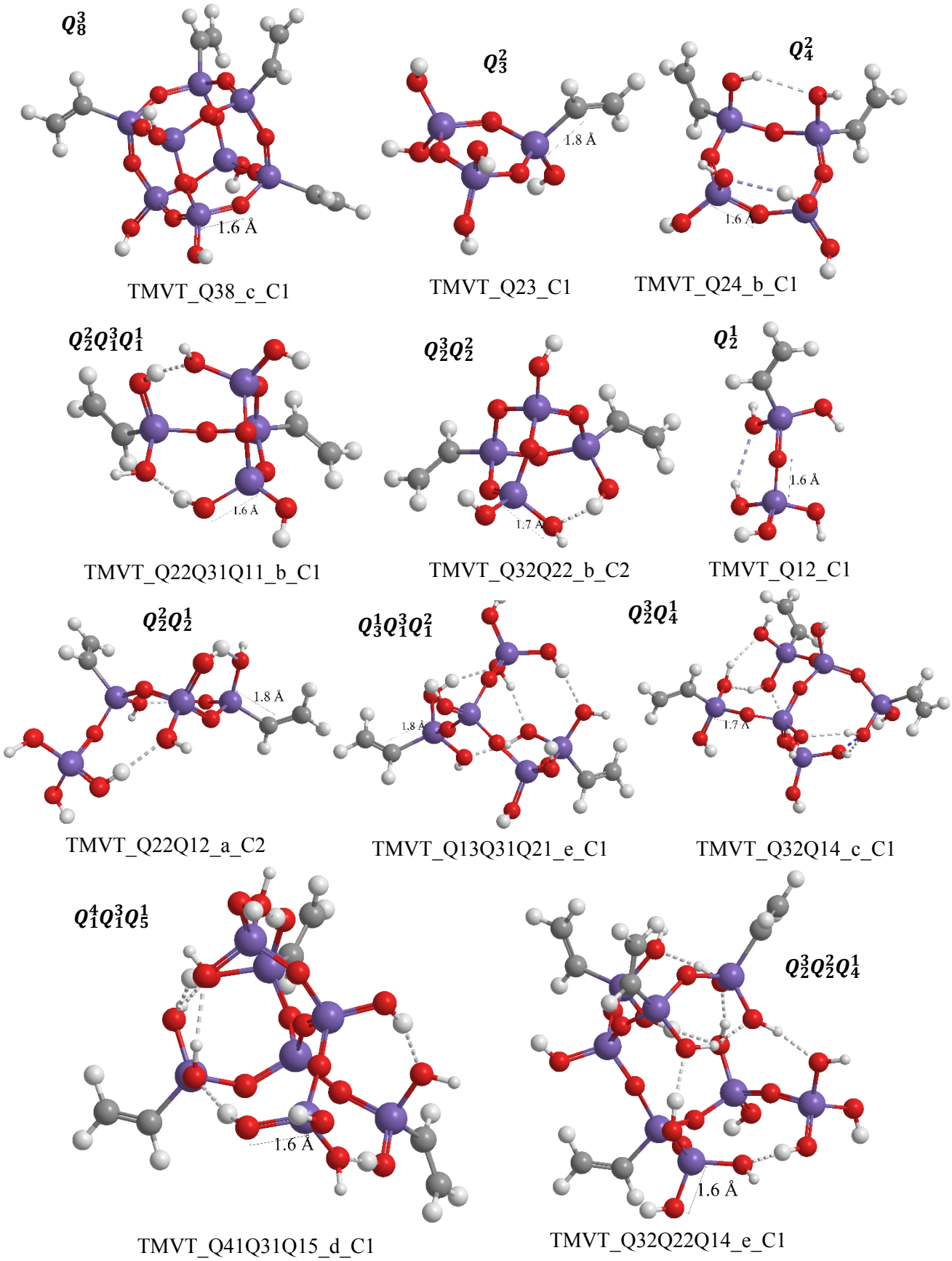

Figure A.1 – B3LYP/6-311+G(d,p) optimized geometries of the most stable silica cluster structures for the 50% TMOS/50% VTMS aerogel. Si atoms in purple, O in red, C in grey and H in white. The length of one bond was added for scale. Dashed lines represent hydrogen bonds.

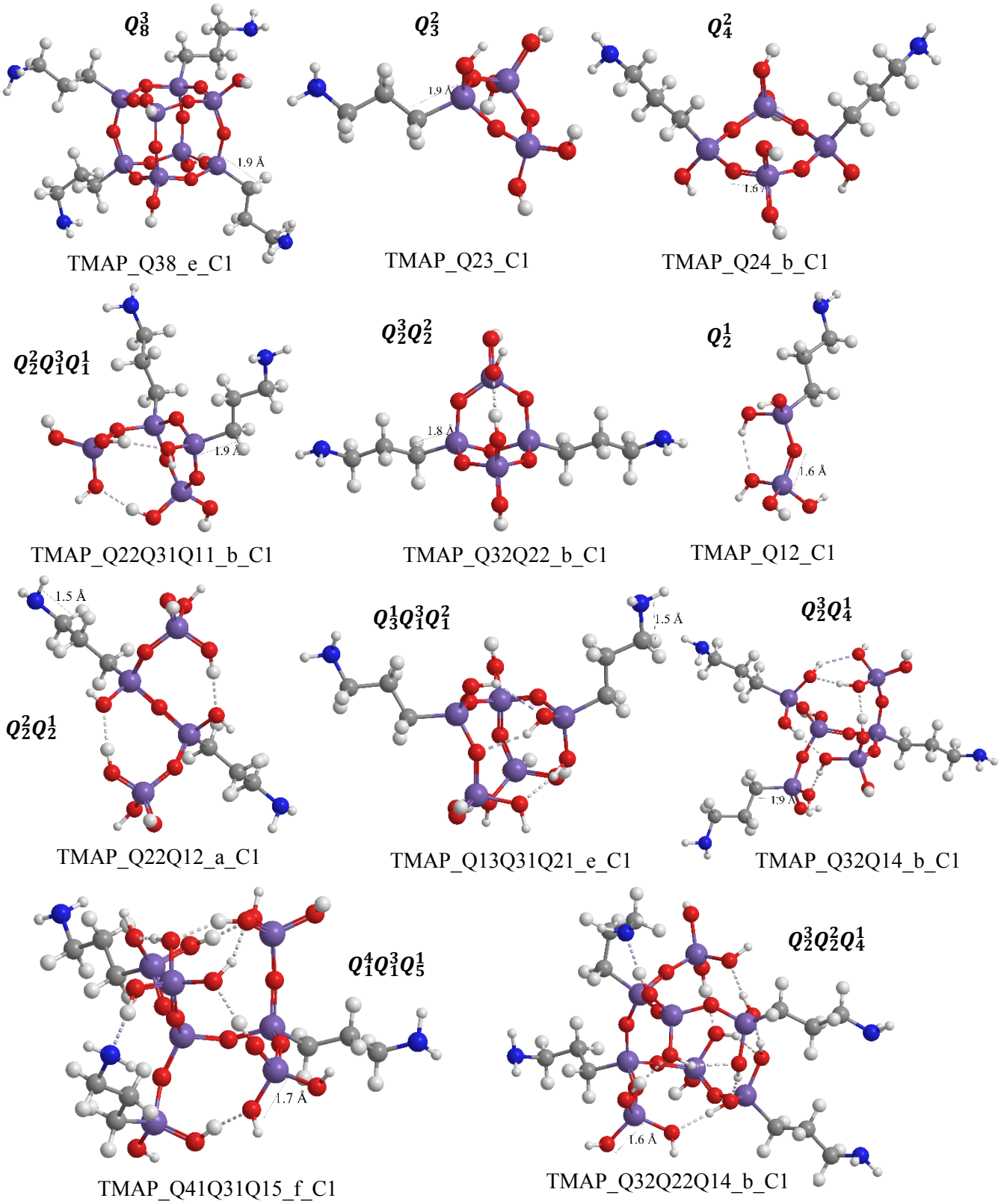

Figure A.2 - B3LYP/6-311+G(d,p) optimized geometries of the most stable silica cluster structures for the 50% TMOS/50% APTMS aerogel. Si atoms in purple, O in red, N in blue, C in grey and H in white. The length of one bond was added for scale. Dashed lines represent hydrogen bonds.

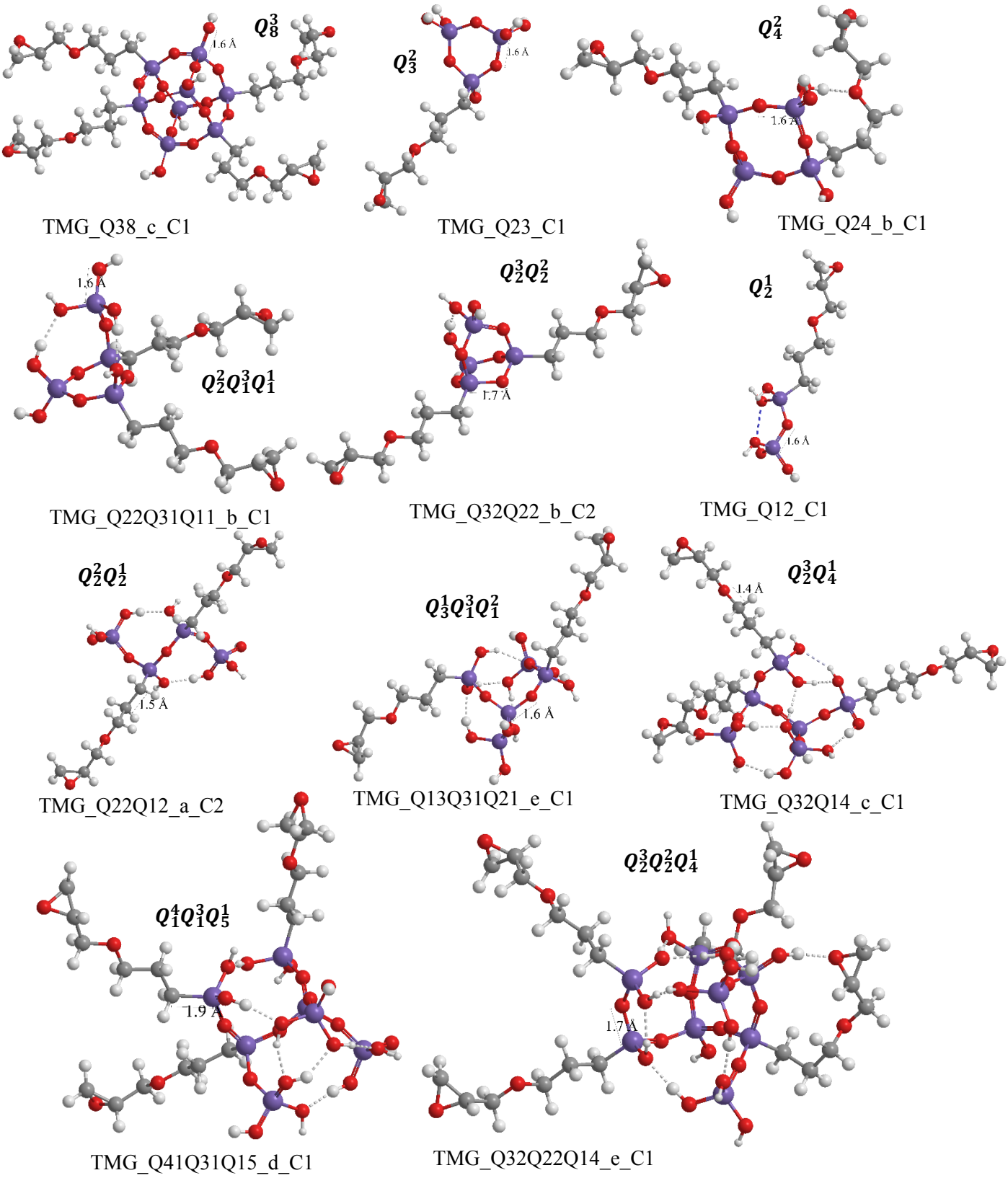

Figure A.3 – B3LYP/6-311+G(d,p) optimized geometries of the most stable silica cluster structures for the 50% TMOS/50% GLYMO aerogel. Si atoms in purple, O in red, C in grey and H in white. The length of one bond was added for scale. Dashed lines represent hydrogen bonds.

Results from spectroscopic analysis

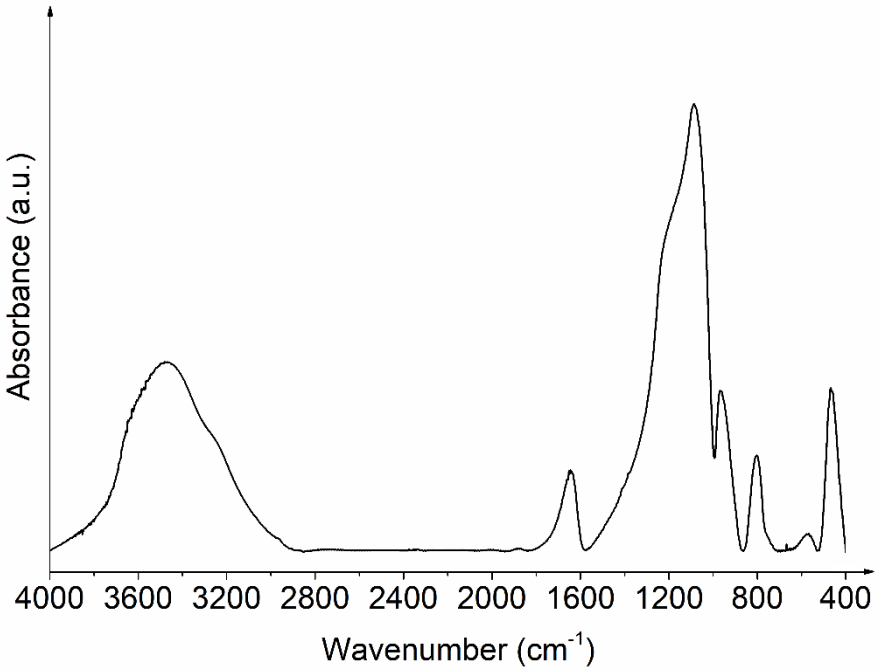

Figure A.4 – Experimental FTIR spectrum of the aerogel synthesized from the precursor TMOS (full frequency range).

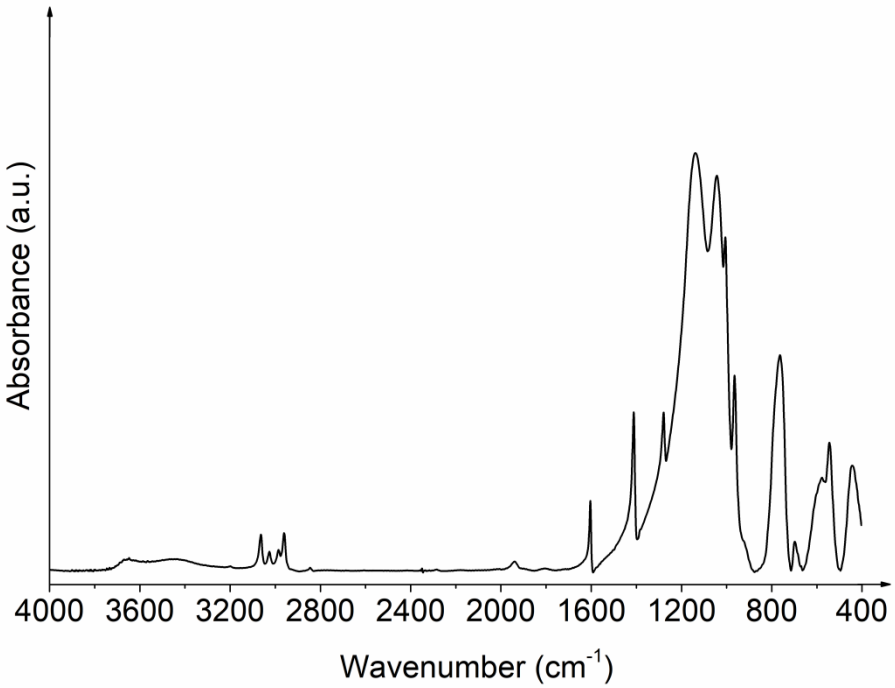

Figure A.5 – Experimental FTIR spectrum of the aerogel synthesized from the precursor VTMS (full frequency range).

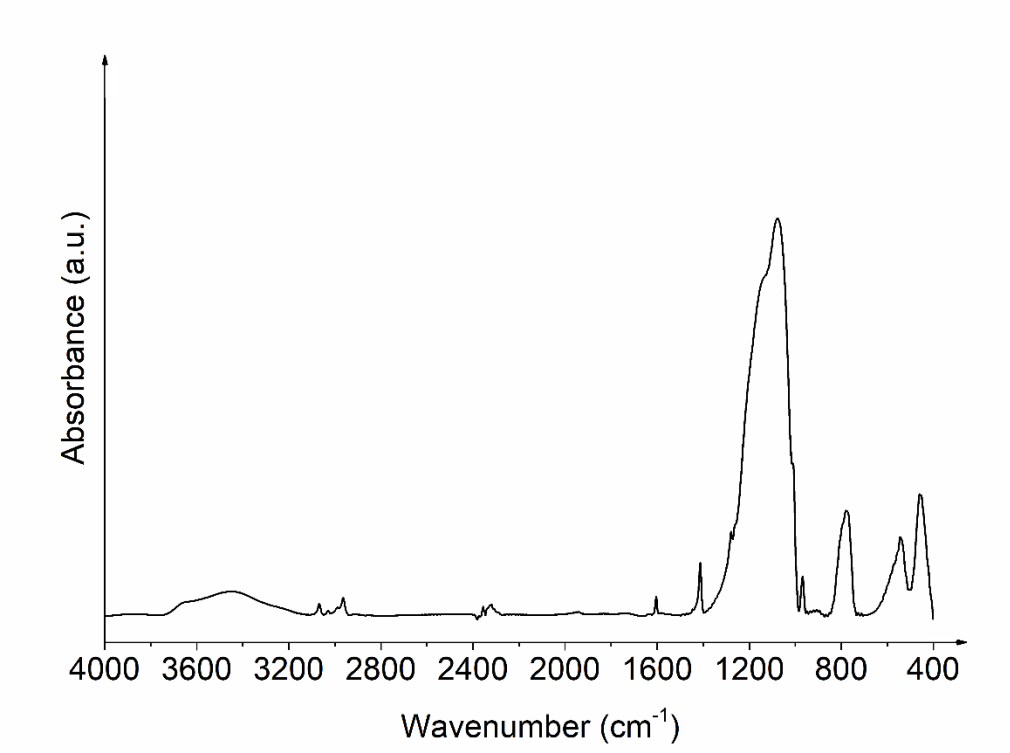

Figure A.6 - Experimental FTIR spectrum of the aerogel obtained from a mixture of 50% TMOS and 50% VTMS (full frequency range).

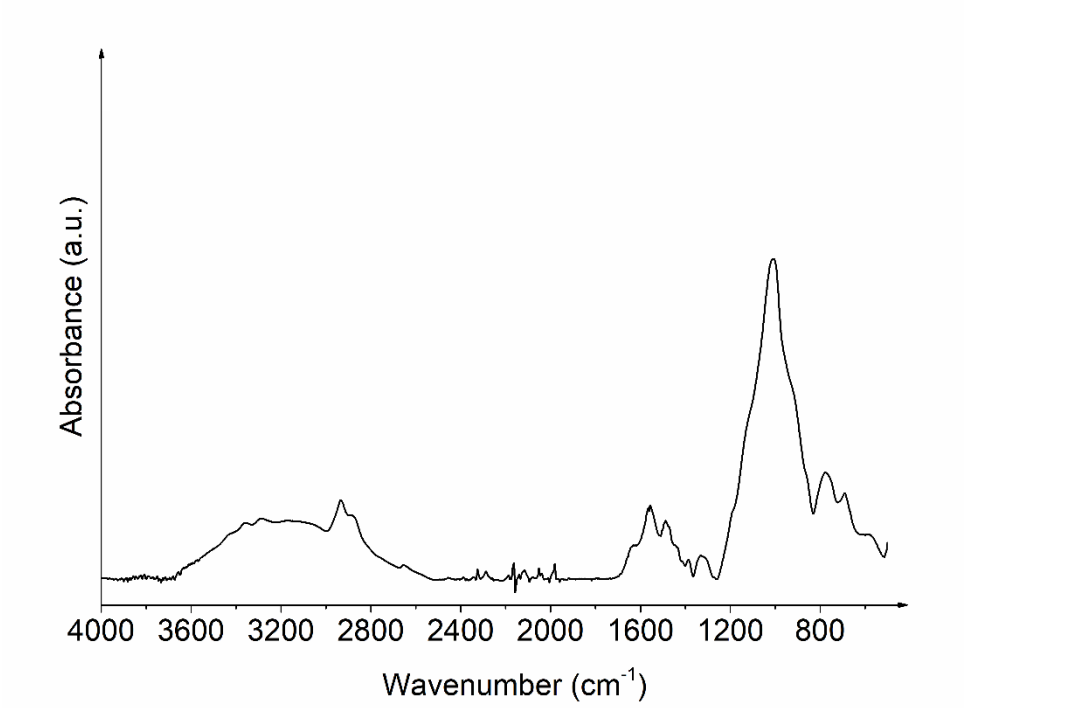

Figure A.7 - Experimental FTIR spectrum of the aerogel obtained from a mixture of 50% TMOS and 50% APTMS (full frequency range).

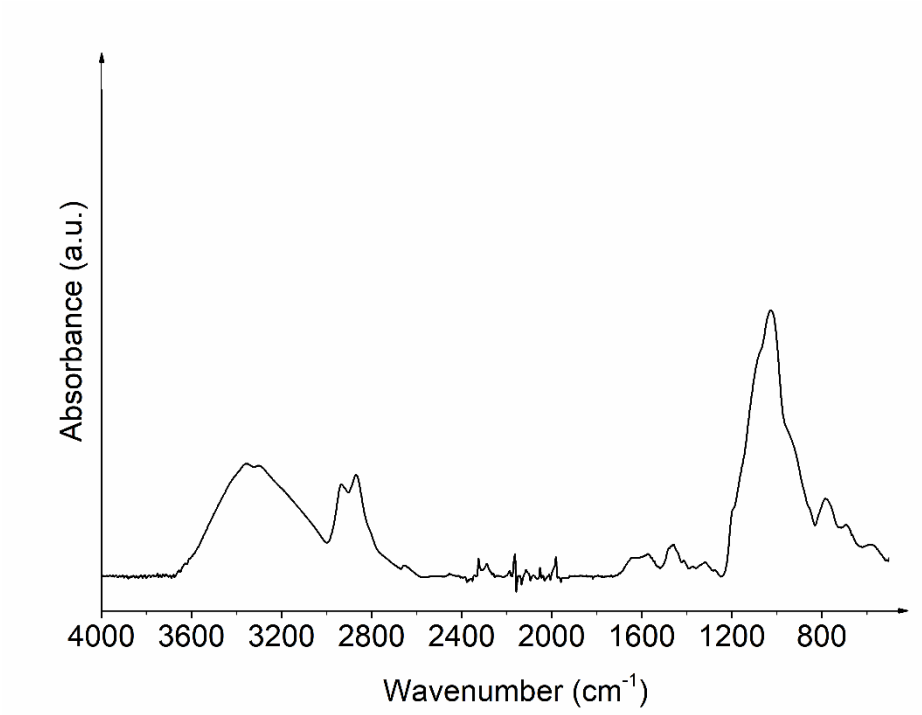

Figure A.8 - Experimental FTIR spectrum of the aerogel obtained from a mixture of 50% TMOS and 50% GLYMO (full frequency range).

Table A.7 – Vibration modes and respective experimental and theoretical frequencies of the IR spectra of the 100% TMOS silica aerogel, in the region 1500 - 400 cm^{-1}.

Vibration mode [a]	**Wavenumber (cm^{-1})**		
	Literature [b]	**Experimental**	**Theoretical**
ν_{as} (Si-O-Si) polycyclic [c]	1200 - 1130	1218 (sh)	1161
ν_{as} (Si-O-Si) cyclic trimers and linear chains	1090 - 1010	1087	1060
δ(O-H)	1040 - 1020		
ν(Si-O)	955 - 830	969	962
ν_s(Si-O-Si) + δ(O-H)	870 - 820	802	810
ν_s(Si-O-Si)	800 - 783	751 (sh)	728
ν(Si-O)	550 - 580	567	587
δ(O-Si-O)	459 - 469	468	474

[a] ν - stretching; ν_s - symmetric stretching; ν_{as} - asymmetric stretching; δ - bending. [b] Refs [1,2]. [c] Includes species with intramolecular hydrogen bonds that form polycyclic-like structures.

Table A.8 – Vibration modes and respective experimental and theoretical frequencies of the IR spectra of the 100% VTMS silica aerogel, in the region 1400 - 400 cm^{-1}.

Vibration mode [a]	**Wavenumber (cm^{-1})**		
	Literature [b]	**Experimental**	**Theoretical**
δ(=C-H)	1330 - 1240	1279	1300
v_{as} (Si-O-Si) polycyclic [c]	1200 - 1130	1139	1124
v_{as} (Si-O-Si) cyclic trimers and linear chains δ(O-H)	1090 - 1010 1040 - 1020	1043	1041
δ(-C**H**=C**H$_2$**)	1010 - 990	1006	[d]
w(H-C-H)	995 - 980	966	[d]
v(Si-OH) + δ(O-H)	955 - 830	919 (sh)	924
v(Si-C)	785 - 805	763	811
v_s (Si-O-Si)	800 - 680	697	745
γ(=C-H)	530 - 540	584 544	635 595
δ(O-Si-O)	459 - 469	441	480

[a] *v* - stretching; v_s - symmetric stretching; v_{as} - asymmetric stretching; δ - bending; γ - twisting; *w* - wagging.

[b] Refs [1,2] [c] Includes species with intramolecular hydrogen bonds that form polycyclic-like structures. [d] These vibration modes are predicted by the quantum mechanics calculations, but have such low intensity that they do not produce a distinct peak in the theoretical spectrum.

Table A.9 - Experimental ^{29}Si-NMR chemical shift assignments to Si environments denoted by the Qx notation (see main text), and theoretically calculated values for all silica clusters of the 100% TMOS aerogel.

Species		Chemical shifts in Si environments (ppm)				
		Q4	**Q3**	**Q2**	**Q1**	**Q0**
Theoretical	Q_8^3	N/A	-115.98 to -115.86	N/A	N/A	N/A
	$Q_4^3Q_4^2$	N/A	-118.81 to -118.36	-106.64 to -106.09	N/A	N/A
	Q_3^2	N/A	N/A	-96.91 to -96.10	N/A	N/A
	Q_4^2	N/A	N/A	-102.03 to -99.72	N/A	N/A
	$Q_2^2Q_1^3Q_1^1$	N/A	-104.97	-95.35 -94.05	-91.82	N/A
	$Q_2^3Q_2^2$	N/A	-96.41 -95.86	-94.28 -93.70	N/A	N/A
	$Q_1^4Q_2^3Q_4^1$	-121.66	-104.85 -104.82	N/A	-95.06 to -90.04	N/A
	Q_2^1	N/A	N/A	N/A	-91.01 -88.55	N/A
	$Q_2^1Q_1^2$	N/A	N/A	-99.17	-94.71 -88.88	N/A
	$Q_3^1Q_1^3$	N/A	-111.29	N/A	-94.14 to -88.05	N/A
	$Q_2^2Q_2^1$	N/A	N/A	-104.51 -98.85	-92.56 -88.64	N/A
	$Q_3^1Q_1^3Q_1^2$	N/A	-115.87	-101.34	-91.90 to -88.03	N/A
	$Q_2^3Q_4^1$	N/A	-121.80 -118.17	N/A	-96.79 to -91.48	N/A
	$Q_1^4Q_1^3Q_5^1$	-128.79	-114.30	N/A	-98.02 to -88.44	N/A
	$Q_2^3Q_2^2Q_4^1$	N/A	-119.43	-103.83	-93.92 -93.32	N/A
	TMOS	N/A	N/A	N/A	N/A	-81.11
Experimental		-109.33	-99.45 -100.40	-90.88	Not observed	Not observed
Literature [b]		-120 a -104	-104 a -94	-96 a -85	-85 a -75	-75 a -66

[a] Chemical shifts relative to tetramethylsilane (TMS). In the case of the theoretical spectra, δ_{Si} (TMS) = 330.18 ppm. [b] Refs [3,4,5]

Table A.10 - Experimental ^{29}Si-NMR chemical shift assignments to Si environments according to the Qx notation (see main text), along with theoretically calculated values for all silica clusters of the VTMS-based aerogel.

Species		Chemical shifts in Si environments (ppm)			
		T3	**T2**	**T1**	**T0**
Theoretical	$\boldsymbol{Q_8^3}$	-93.51	N/A	N/A	N/A
	$\boldsymbol{Q_4^3Q_4^2}$	-90.24 -89.77	-79.77 -77.96	N/A	N/A
	$\boldsymbol{Q_3^2}$	N/A	-75.80 -75.28	N/A	N/A
	$\boldsymbol{Q_4^2}$	N/A	-75.91 -74.47	N/A	N/A
	$\boldsymbol{Q_2^2Q_1^3Q_1^1}$	-82.09	-74.08 -71.57	-70.62	N/A
	$\boldsymbol{Q_2^3Q_2^2}$	-72.01	-69.12	N/A	N/A
	$\boldsymbol{Q_2^1}$	N/A	N/A	-71.98 -72.16	N/A
	$\boldsymbol{Q_2^1Q_1^2}$	N/A	-81.16	-67.45 -67.07	N/A
	$\boldsymbol{Q_3^1Q_1^3}$	-88.44	N/A	-67.36 to -66.84	N/A
	$\boldsymbol{Q_2^2Q_2^1}$	N/A	-78.11	-66.43	N/A
	$\boldsymbol{Q_3^1Q_1^3Q_1^2}$	-93.21	-75.00	-70.23 to -63.83	N/A
	$\boldsymbol{Q_2^3Q_4^1}$	-100.65 -96.46	N/A	-74.02 to -69.48	N/A
	$\boldsymbol{Q_2^3Q_2^2Q_4^1}$	-91.97	-77.53	-70.40 -64.99	N/A
	VTMS	N/A	N/A	N/A	-59.48
Experimental		-77.89 -78.56	-69.56	Não observável	Não observável
Literature [b]		-81 a -76	-72 a -66	-63 a -59	-59 a -50

[a] Chemical shifts relative to tetramethylsilane (TMS). In the case of the theoretical spectra, δ_{Si} (TMS) = 330.18 ppm. [b] Refs [3,4,5]

Experimental details

The infrared (IR) spectra of aerogels synthesized from 100% TMOS, 100% VTMS and 50% TMOS/50% VTMS were obtained with KBr pellets in a Jasco FTIR 4200 Fourier transform infrared (FTIR) spectrometer, in the range of 4000 to 400 cm^{-1}, with a resolution of 4 cm^{-1} and 128 scans, equipped with a Deuterated Lanthanum α-Alanine doped TriGlycine Sulphate (DLaTGS) detector and a Ge/KBr beamsplitter. On the other hand, the IR spectra corresponding to aerogels derived from mixtures of 50% TEOS/50% APTES and 50% TEOS/50% GLYMO was obtained by Attenuated Total Reflectance-FTIR (ATR-FTIR), in the range 4000-500 cm^{-1} with a

resolution of 4.0 cm^{-1} and 256 scans, using a Frontier - Perkin Elmer Fourier transform infrared spectrometer (FT-NIR/MIR), equipped with an electrically temperature-stabilized fast recovery deuterated triglycine sulfate (FR-DTGS) detector, a KBr beamsplitter and a Specac MKII Golden Gate ATR module, with a 45° and 2 mm × 2 mm diamond crystal. Due to the complexity of the IR spectra in the region corresponding to the largest peak (1500-1000 cm^{-1}) for the aerogels with heterogeneous composition (*i.e.* mixtures of 50% TMOS/50% VTMS, 50% TEOS/50% APTES and 50% TEOS/50% GLYMO), the spectra were deconvoluted using Voigt functions fitted via the Levenberg-Marquardt algorithm.

The solid-state ^{29}Si NMR spectra of all samples were obtained using a Varian 500WB spectrometer and a 5 mm PENCIL™ probe, with cross-polarization and magic angle spinning (MAS) with a frequency of 11 kHz.

References

[1] G. Socrates, Infrared and Raman Characteristic Group Frequencies: Tables and Charts, Wiley, 2001.

[2] R. Al-Oweini, H. El-Rassy, Synthesis and characterization by FTIR spectroscopy of silica aerogels prepared using several $Si(OR)_4$ and $RSi(OR)_3$ precursors, Journal of Molecular Structure (1) (2009) 140 – 145.

[3] A. Borba, J. P. Vareda, L. Durães, A. Portugal, P. N. Simões, Spectroscopic characterization of silica aerogels prepared using several precursors – effect on the formation of molecular clusters, New J. Chem. 41 (2017) 6742 – 6759.

[4] O. Filonenko, V. Kuts, M. Terebinska, V. Lobanov, Quantum-chemical calculation of 29 Si NMR spectrum of silicon dioxide fullerene-like molecules, Himia, Fizika ta Tehnologia Poverhni 6 (2) (2015) 263 – 268

[5] J. Šefčik, A. McCormick, Kinetic and thermodynamic issues in the early stages of sol-gel processes using silicon alkoxides, Catalysis Today 35 (3) (1997) 205 – 223, sol-gel Preparation of Catalytic Materials.

[6] B. N. Nguyen, M. A. B. Meador, M. E. Tousley, B. Shonkwiler, L. McCorkle, D. A. Scheiman, A. Palczer, Tailoring elastic properties of silica aerogels cross-linked with polystyrene, ACS Applied Materials & Interfaces 1 (3) (2009) 621 – 630